Environmental Fluid Mechanics **1:** 171–208, 2001.

Numerical Investigation of Boundary-Layer Evolution and Nocturnal Low-Level Jets: Local versus Non-Local PBL Schemes

KESU ZHANG[a], HUITING MAO[a], KEVIN CIVEROLO[b], STEPHEN BERMAN[c], JIA-YEONG KU[b], S. TRIVIKRAMA RAO[a,b,*], BRUCE DODDRIDGE[d], C. RUSSELL PHILBRICK[e] and RICHARD CLARK[f]
[a]*University at Albany, Department of Earth and Atmospheric Sciences, Albany, NY, U.S.A.*
[b]*New York State Department of Environmental Conservation, Albany, NY, U.S.A.*
[c]*College at Oneonta, Earth Sciences Department, Oneonta, NY, U.S.A.*
[d]*University of Maryland, Department of Meteorology, College Park, MD, U.S.A.*
[e]*Pennsylvania State University, Department of Electrical Engineering, University Park, PA, U.S.A.*
[f]*Millersville University, Department of Earth Sciences, Millersville, PA, U.S.A.*

Received 10 November 2000; accepted in revised form 23 February 2001

Abstract. Numerical simulations of the evolution of the planetary boundary layer (PBL) and nocturnal low-level jets (LLJ) have been carried out using MM5 (version 3.3) with four-dimensional data assimilation (FDDA) for a high pollution episode in the northeastern United States during July 15–20, 1999. In this paper, we assess the impact of different parameterizations on the PBL evolution with two schemes: the Blackadar PBL, a hybrid local (stable regime) and non-local (convective regime) mixing scheme; and the Gayno–Seaman PBL, a turbulent kinetic energy (TKE)-based eddy diffusion scheme. No FDDA was applied within the PBL to evaluate the ability of the two schemes to reproduce the PBL structure and its temporal variation. The restriction of the application of FDDA to the atmosphere above the PBL or the lowest 8 model levels, whichever is higher, has significantly improved the predicted strength and timing of the LLJ during the night. A systematic analysis of the PBL evolution has been performed for the primary meteorological fields (temperature, specific humidity, horizontal winds) and for the derived parameters such as the PBL height, virtual potential temperature, relative humidity, and cloud cover fraction. There are substantial differences between the PBL structures and evolutions simulated by these two different schemes. The model results were compared with independent observations (that were not used in FDDA) measured by aircraft, RASS and wind profiler, lidar, and tethered balloon platforms during the summer of 1999 as part of the NorthEast Oxidant and Particle Study (NE-OPS). The observations tend to support the non-local mixing mechanism better than the layer-to-layer eddy diffusion in the convective PBL.

Key words: Blackadar PBL, Gayno–Seaman PBL, low-level jets, meteorological modeling, MM5, planetary boundary layer

1. Introduction

Planetary boundary layer (PBL) structure and its evolution play a vital role in the physical and chemical processes occurring in the atmosphere, including cloud-

*Corresponding author, E-mail: strao@dec.state.ny.us

radiation interactions, nocturnal transport, and vertical mixing. Such processes directly affect the formation, transport, and removal of ozone (O_3), fine particulate matter ($PM_{2.5}$), and their precursors in the atmosphere. During the daytime, the PBL is generally well-mixed, and vertical profiles of pollutants and other scalar quantities are fairly uniform throughout the mixed layer. At nighttime, the near-surface and residual layers become decoupled, and the pollutants trapped aloft in the residual layer are transported to long distances via low-level jets (LLJs); this can greatly affect ground-level pollutant concentrations downwind of the source region on the following day. Hence, a more thorough understanding of the PBL evolution and its underlying dynamics is the first step to a more accurate formulation of a PBL scheme. This, in turn, should lead to improved numerical modeling and a better understanding of the key boundary layer processes that affect the distribution of pollutant concentrations.

Since the twice-a-day soundings are not sufficient to provide useful information for studying the PBL evolution over the diurnal cycle, remote sensing measurements such as Doppler wind profilers, radio acoustic sounding system (RASS) temperature profilers, and lidar have increasingly been used for PBL detection (for example, see [1] and references therein). These nearly continuous measurements will greatly help improve our understanding of the PBL structure and its temporal evolution, and ability to evaluate numerical models. However, such resource-intensive measurements cannot provide the wide spatial coverage that a sounding network does. To investigate the dynamical features and identify the real physical processes in the PBL, grid-based numerical models become necessary; such models are able to integrate the isolated observations into a dynamically-consistent framework via four-dimensional data assimilation (FDDA) techniques. Over the past decade, mesoscale atmospheric models have been used to provide 'surrogate data' for mesoscale analysis on time scales of less than one day.

Despite success in the simulation of synoptic processes, dynamical models are far less capable of simulating sub-grid scale features, such as cloud-precipitation processes and PBL evolution, because too many semi-empirical parameterizations are involved. The object of this study is to test and compare two existing PBL schemes with FDDA capability in the Fifth-Generation Penn State/NCAR Mesoscale Model Version 3.3 (MM5V3; available from the NCAR Mesoscale and Microscale Meteorology Division website: http://www.mmm.ucar.edu/mm5/mm5-home.html), which is being used in air quality modeling studies. A recent paper [2] evaluated these two PBL schemes based on numerical simulations of the mid-July 1991 period for the Lake Michigan Ozone Study (LMOS). However, their results may not be conclusive because the effects of the modified FDDA were not fully investigated for the Blackadar PBL. Alapaty *et al.* [3] tested two local and two non-local PBL schemes with a one-dimensional model. They found that the main differences occurred in the surface layer and near the top of the mixed layer. A more comprehensive evaluation of the different PBL schemes requires the combined simulation of PBL processes and associated mesoscale circulations in three-dimensional models.

This paper describes parallel simulations using MM5V3, with local and non-local PBL schemes, both with and without modified FDDA. The objects of these simulations are to evaluate a 'state-of-the-science' meteorological model in terms of our knowledge of the boundary layer dynamical processes; to generate the necessary inputs for a corresponding air quality model simulation for this episode (Ku *et al.*, [4]); and to investigate how the uncertainties in the meteorological modeling results affect the predicted pollutant concentrations. Comparisons between model outputs and independent observations taken for an O_3 and $PM_{2.5}$episode during July 15–20, 1999 have been performed to identify the PBL scheme that more closely describes the 'real' mixing processes in the PBL. The meteorological model and the two PBL schemes are described in Sections 2 and 3, respectively. The independent observations used to help evaluate the modeling system are reported in Section 4. The synoptic features of the July 1999 episode are briefly discussed in Section 5. The PBL evolution and comparison with observations are discussed in Section 6, while comparisons between observations and predictions of LLJs are presented in Section 7. Finally, a general statistical evaluation of model performance is given in Section 8.

2. The Meteorological Model (MM5V3)

The model used for the current PBL study is the non-hydrostatic, primitive equation, mesoscale model developed by PSU/NCAR, known as MM5 [5, 6]. The beta-release of MM5 version 3.3 (MM5V3), containing additional options for physics, enables the numerical modeling community to use it for various research and application purposes. The model includes a soil module, seven PBL schemes, and eight microphysics schemes, with different degrees of complexity.

In the original simulations, FDDA was applied to the free atmosphere (above the diagnosed PBL height) for a 5-day simulation covering July 15–20, 1999. When a dynamical model is used as a driver for photochemical models such as MODELS-3 [7], FDDA is necessary for correctly reproducing the synoptic forcing above the PBL over longer time scales (>3–5 days). Applications of FDDA to MM5 are common in many air quality studies [2, 8–12]. However, it is inappropriate to apply FDDA in the PBL because insufficient observations may obscure the diurnal evolution and PBL structure. Therefore, we have limited FDDA to above the PBL in order to assess the ability of the two PBL modules, namely the Blackadar scheme (BLPBL; [13]) and Gayno–Seaman scheme (GSPBL; [14]), in reproducing the PBL, by focusing only on the model's physical processes. Since these PBL schemes can be used by MM5V3 to generate the necessary meteorological fields needed for a subsequent air quality simulation, it is important to identify the strengths and weaknesses of the two PBL schemes.

The model configuration is a triply-nested domain having horizontal grid resolutions of 108/36/12 km, respectively, for all experiments (Figure 1). Also shown in Figure 1 are the approximate locations of two vertical cross-sections that will be

Table I. The vertical structure used in the MM5V3 simulations. The non-dimensional pressure (σ) levels, approximate pressure (mb), approximate height (m AGL), approximate layer thickness (m), and ratio of adjacent layer thickness is shown.

Model level	σ level	Pressure (mb)	Approximate mid-layer height (m AGL)	Layer thickness, dz (m)	Ratio of dz[a]
25	0.9987	1019	10	20	1.93
24	0.9937	1014	48	39	1.75
23	0.985	1006	116	67	1.74
22	0.97	992	233	117	1.52
21	0.9475	972	411	178	1.36
20	0.9175	944	654	243	1.28
19	0.88	910	965	312	1.17
18	0.8375	871	1331	365	1.10
17	0.7925	829	1732	402	1.04
16	0.7475	788	2151	419	1.10
15	0.70	744	2613	462	1.11
14	0.65	698	3124	511	1.06
13	0.60	652	3664	540	1.06
12	0.55	606	4236	572	1.07
11	0.50	560	4845	609	1.08
10	0.45	514	5497	652	1.08
9	0.40	468	6199	702	1.09
8	0.35	422	6960	761	1.10
7	0.30	376	7793	833	1.11
6	0.25	330	8715	922	1.12
5	0.20	284	9749	1034	1.14
4	0.15	238	10932	1183	1.20
3	0.10	192	12348	1416	1.28
2	0.05	146	14154	1806	0.98
1	0.0125	112	15931	1777	N/A

[a]The ratio of adjacent layer thickness is kept between 1–2 to avoid numerical reflection.

discussed later in this paper: a west-to-east cross-section through the 12-km domain (near 40° N; 'W-E') and a cross-section through Philadelphia, PA and southern NJ ('NJ'). In the vertical, 25 terrain-following surfaces are designated by the non-dimensional pressure levels (σ) listed in Table I. Also shown in Table I are the pressure, mid-layer height, layer thickness (dz), and the ratio of adjacent layers, which varies between 1 and 2 to avoid sudden changes and possible numerical reflection. This resolution may not be sufficient to resolve sharp changes in the surface layer or near the top of the mixing layer or shallow inversion layer, and may

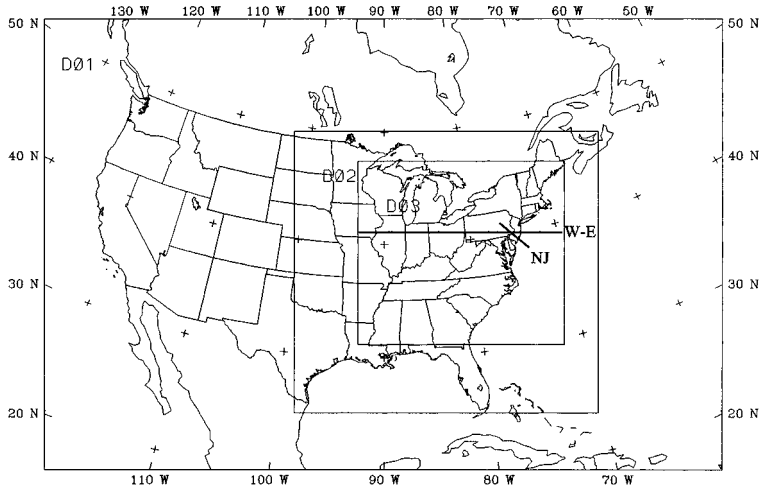

Figure 1. The triply-nested MM5V3 modeling domain with the 108 km (D01), 36 km (D02), and 12 km (D03) horizontal grid structure. The line denoted 'NJ' is the New Jersey cross-section, and the line denoted 'W–E' is the west-to-east cross-section through the 12-km domain (near 40°N), both through Philadelphia, PA.

not adequately resolve LLJs. With increasing computer power, it may be possible to increase the vertical resolution throughout the PBL to 100 m or less in the future.

The model parameters and physics options used in the 12 km domain, summarized in Table II, strongly influence the physical processes and evolution of the PBL, and the FDDA processes. The two original experiments are identical except for the use of two different PBL schemes. All other physics modules, namely, the long- and shortwave radiation, cloud fraction diagnosis, simple ice microphysics, ground temperature energy balance equation, surface layer parameterization, deep cumulus parameterization, and shallow convection scheme, are common to both sets of the original simulations.

In the original simulations, the effects of FDDA on the lower atmosphere are most pronounced at night after the collapse of the PBL, while during the afternoon the diagnosed PBL height is usually 1–2 km above ground level and no FDDA has been applied within it. However, at nighttime when the PBL collapses, MM5V3 sets the PBL height to the lowest model layer, and the effects of FDDA can be felt near the surface. If one is to successfully simulate the diurnal evolution of the PBL and nocturnal transport via LLJs, which can have core wind speeds on the order of 10–15 m s^{-1} around 300-800 m above ground level (AGL), the synoptic-scale nudging effects must be removed to focus only on the model dynamics for LLJ formation. To reduce the nighttime effects of the FDDA, we also performed two sets of modified simulations in which we attempted to investigate the LLJ formation through dynamical processes alone in the model. For the modified LLJ experiments, FDDA was further restricted to above the height of the PBL (mainly

Table II. Model parameters and settings used in the MM5V3 12 km grid domain.

Parameters	MM5V3 (BLPBL)	MM5V3 (GSPBL)
12 km domain (N_x, N_y, N_z)	(166,148,25)	(166,148,25)
Dynamics in the vertical	Non-hydrostatic	Non-hydrostatic
Upper boundary	Radiative condition	Radiative condition
Lateral boundary condition from the 36 km domain	2-way nesting	2-way nesting
Short- and long-wave radiation?	Yes	Yes
PBL scheme	Blackadar	Gayno–Seaman
PBL height	θ_v-profile (PBL where NE = 0.2 × PE for CPBL)	TKE-profile (PBL where TKE = 0.1 m^2 s^{-2})
Vertical mixing in the CPBL	Non-local mixing (symmetric)	K-theory (local eddy diffusion) K_v = f(l,N,S,h,TKE)
Ground temperature (T_g)	Slab energy balance equation	Slab energy balance equation
Surface fluxes over 13 land categories	Monin–Obukhov similarity theory	Monin–Obukhov similarity theory
Cumulus precipitation?	No	No
Grid-resolvable precipitation	Warm rain and simple ice scheme	Warm rain and simple ice scheme
Shallow convection?	Yes	Yes
Upper air 3D-FDDA?	Yes	Yes
2D surface FDDA?	Yes	Yes
FDDA in PBL?	No	No

during the daytime) or the lowest 8 model levels (about 1.3 km, mainly during nighttime hours), whichever is higher.

3. Local and Non-Local PBL Schemes in MM5V3: Blackadar PBL versus Gayno–Seaman PBL

While there are seven different PBL formulations in MM5V3, only the Hong-Pan ('MRF') [15, 16], BLPBL, and GSPBL schemes have FDDA capability. In this

analysis, we focus only on the latter two PBL schemes, because they have an identical formulation for the surface fluxes. The formulation of the BLPBL can be found in Blackadar [13], Zhang and Anthes [17], and Grell *et al.* [6], while the GSPBL and its application in meteorological models are described in Gayno *et al.* [14] and Shafran *et al.* [2]. Since the overall characteristics of these two PBL schemes have already been documented [2], this analysis focuses on identifying the scheme that best reproduces the mixing heights and vertical exchange processes.

The PBL height determined by different schemes can vary widely even when diagnosed from the same temperature and wind fields, let alone from different meteorological sources. In MM5V3, the PBL is classified into four stability cases: (1) stable, (2) wind shear-driven turbulence, (3) forced convection, and (4) unstable free convection. These stability classes are based on the following parameters: the bulk Richardson number of the surface layer, and $|h/L|$, where h is the PBL height and L is the Monin–Obukhov length. The first two cases are in the stable regime, while the latter two cases are in the convective regime.

The Blackadar scheme distinguishes the stable and unstable PBL regimes according to the bulk Richardson number of the surface layer ($\mathrm{Ri}_{\mathrm{sfc}}$) only. For the two stable cases ($\mathrm{Ri}_{\mathrm{sfc}} > 0$), the PBL height is artificially set to the lowest model layer [17]. The two unstable cases ($\mathrm{Ri}_{\mathrm{sfc}} < 0$), forced and free convection, are distinguished by the parameter $|h/L|$; for the forced convection case $|h/L| < 1.5$, and $|h/L| > 1.5$ for the free convection case. For the forced convection case, the BLPBL sets the PBL height to the level where the virtual potential temperature (θ_v) exceeds θ_v in the surface layer. For the free convective PBL, the BLPBL computes the buoyant energy within the whole PBL, then defines the mixing layer height as the level above which the negative energy reaches 20% of the total positive energy (i.e., allows for 'over-shooting'). This non-local method is based upon the integrated thermal structure of the θ_v profile. For the stable and forced convective regimes, vertical mixing in the BLPBL relies on so-called 'K-theory'. Hence, the BLPBL is a hybrid local and non-local scheme, in which a first-order eddy diffusivity (K), a function of the local Richardson number, is applied to the stable and forced convective cases, while non-local mixing between the surface layer and all the other layers is used for the unstable free convective PBL. In some instances, the PBL regime can change abruptly, leading to a rapid shift between local and non-local vertical exchange.

The GSPBL computes K from the local gradients in turbulent kinetic energy (TKE), vertical wind shear and stability, and the Blackadar length scale [2], regardless of stability regime. The TKE is the only second moment predicted by the model. The scheme that includes both first-order and second-order moments can be considered a '1.5-order closure' scheme. During convective periods, the GSPBL defines the PBL height as the level where the TKE drops below a critical threshold of 0.1 $\mathrm{m}^2\ \mathrm{s}^{-2}$ if the maximum TKE is larger than 0.2 $\mathrm{m}^2\ \mathrm{s}^{-2}$ (strong convection); otherwise, when the maximum TKE is less than 0.2 $\mathrm{m}^2\ \mathrm{s}^{-2}$ (weak convection), the PBL height is set to the level where the TKE decreases by 50%

of its maximum value. Although not shown here, there were periods when the maximum TKE exceeded 1.5 m^2 s^{-2}; thus, during these times, the PBL height was set to the level where the TKE decreased to about 7% (0.1 m^2 s^{-2}) of the maximum value. Finally, in the case of very weak turbulence (TKE $<$ 0.04 m^2 s^{-2}), such as at night, the PBL height is set to the lowest full model layer.

4. Observations

For the evaluation of model performance, we compared the hourly model predictions from July 15–20 with all hourly surface observations, using the NCAR Data Support Section dataset d470.0, available from the following web address: http://dss.ucar.edu/datasets/ds470.0/. This dataset consists of airport, sounding, National Weather Service, U.S. Navy, U.S. Air Force, and shipboard data. We included all available data located within the 12 km model domain – 396 stations reported temperature and winds, while 284 stations reported humidity.

To evaluate the MM5V3 simulations in terms of the PBL structure and its temporal evolution, we used several sets of remote sensing and in-situ observations. During the summer of 1999, the participants in the NE-OPS project Philbrick [18] collected a suite of meteorological and chemical data at the surface and aloft at a site located at the Baxter Water Treatment Plant in Philadelphia, PA, hereafter referred to as the 'Baxter site'. In addition to the primary surface site, aircraft transects and spirals were performed in the surrounding region, including Northeast Philadelphia Airport (PNE) and Tipton Airport, Ft. Meade, MD (FME). The spirals were generally from near the surface to about 2.7 km AGL, with an approximate ascent rate of 100 m min^{-1}. For model evaluation purposes, we included the following sets of observations in our analysis for the period of July 15–20, 1999:

(a) Remotely-sensed lidar profiles of temperature and water vapor at the Baxter site, measured by the Pennsylvania State University.
(b) Aircraft spirals (diameter ∼5 km) of T and relative humidity (RH) over PNE and FME, measured by the University of Maryland.
(c) Doppler wind and RASS temperature profiler measurements from Ft. Meade (operated by Maryland Department of the Environment), the Baxter site (operated by Pacific Northwest National Laboratory), and Stow, MA (operated by Massachusetts Department of Environmental Protection).
(d) Tethered balloon-based observations of T, RH, and winds to ∼300 m, measured by the Millersville University.

5. Synoptic Features of the July 1999 Episode

Many physical processes impact the PBL structure and evolution, which, in turn, affect our ability to predict pollutant concentrations. These include synoptic-scale

flows, cloud-radiation interactions, land-sea interactions, surface layer processes, and vertical exchange within the PBL. The diurnal variation of the PBL is mainly a result of its response to the thermal and frictional forcing from below. The day-to-day variation of the diurnal cycle, on the other hand, reflects the synoptic forcing from above through variations in cloud-radiation and other dynamical processes. Clearly, then, it is important to characterize the synoptic features. In this section, we briefly present the synoptic features for the period of interest, a mid-July 1999 O_3 and $PM_{2.5}$ episode.

5.1. OBSERVED FEATURES OF THE JULY 15–19, 1999 EPISODE

During the period of July 15–19, 1999 the eastern United States was under the influence of a high-pressure system over land. High temperatures, strong short-wave radiation, and westerly flow dominated the mid-Atlantic and northeastern U.S. region; these conditions are favorable for the transport of pollutants from the Midwest to the East as well as the in-situ formation of ozone and other pollutants. The Appalachian lee trough [19] persisted for three days (July 16–19). This is a typical pressure pattern for high ozone episodes and for the occurrence of LLJs in the northeastern U.S. Along the Atlantic seaboard, the lee trough brought southwesterly flow from the mid-Atlantic region to the northeastern U.S. Large north-south pressure gradients above 37°N helped support westerly low-level flow from the Midwest to the Northeast. This pattern persisted until a cold front passed through the eastern U.S. on July 19.

5.2. GENERAL FEATURES IN THE ORIGINAL MM5V3 SIMULATIONS: TEMPERATURE AND WIND FIELDS

Any differences between the BLPBL- and GSPBL-predicted surface wind and temperature fields are mostly due to the surface forcing resulting from the FDDA, rather than simply from the different physical formulations of the two PBL schemes. Figures 2a and 2b depict the simulated temperature fields at a height of 411 m AGL, at 1800 UTC on July 17 from the BLPBL and GSPBL schemes, respectively. We chose 411 m (fifth level above the surface) because data at this level are more representative of the mixing processes in the PBL than are the surface values. Unless specified, all heights will be reported as AGL in the subsequent sections. The BLPBL scheme predicted a high temperature region (above 28 °C) along the Atlantic seaboard, extending from northern VA to ME, while the GSPBL scheme only predicted a few isolated spots above 28 °C. In the northwestern parts of the 12 km domain, the temperature differences are generally less than about 1 °C. In the southwestern regions of the domain, the BLPBL predictions exceeded the GSPBL predictions by about 2 °C. The two sets of model predictions also tended to deviate along the Atlantic coast (such as Long Island Sound) and around the Great Lakes;

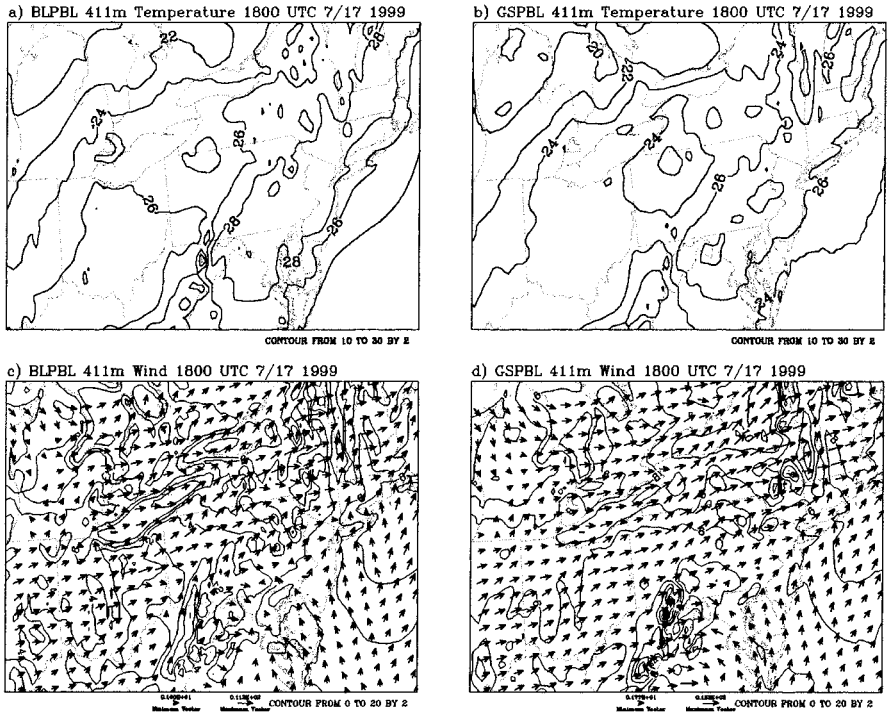

Figure 2. The simulated temperature fields at 1800 UTC, or winds at 1800 UTC on July 17, at about 411 m AGL: (a) BLPBL temperature fields; (b) GSPBL temperature fields; (c) BLPBL wind fields; and (d) GSPBL wind fields.

strong gradients near the surface (not shown) in these regions are responsible for driving the sea and lake breeze circulations.

Figures 2c and 2d show the wind fields at the 411 m height, at 1800 UTC on July 17 as simulated by the BLPBL and GSPBL schemes, respectively. The near-stagnation region, identified by the 2 m s^{-1} isotach, is larger in the BLPBL simulation than in the GSPBL simulation. The GSPBL scheme generated slightly larger wind speeds in the northern and western areas of the 12 km domain. As with the temperature fields, the wind fields also tended to differ between the two simulations along the coastal and lake regions, with larger wind speed gradients predicted by the BLPBL. Also, in the mid-Atlantic region near Philadelphia or over the Long Island Sound, the wind direction is more southerly in the BLPBL simulation. These differences in wind direction will certainly affect pollutant transport along the Atlantic coast.

5.3. CLOUD COVER FRACTION

Since the predicted ground temperature and PBL height in a dynamical model, as well as photochemical kinetic rates in a chemical model, depend upon the short-

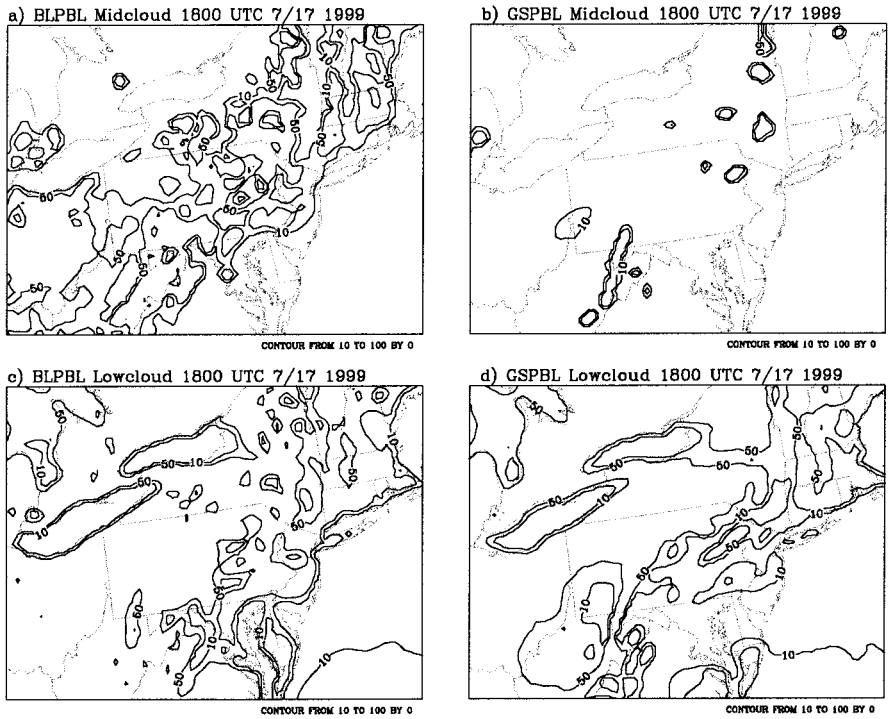

Figure 3. Simulated cloud cover fraction by the two PBL schemes at 1800 UTC on July 17: (a) BLPBL, mid-level clouds; (b) GSPBL, mid-level clouds; (c) BLPBL, low clouds; and (d) GSPBL, low clouds.

wave radiation reaching the ground, an accurate estimation of cloud cover is essential to the thermal and photochemical processes occurring within the PBL. MM5V3 assumes a highly parameterized relationship between cloud cover and RH: the percentage of cloud cover is proportional to the difference between the ambient RH and a critical value RH_c, where RH_c is 60% for high clouds, and 75% for mid-level and low clouds. Walcek [20] compared six different formulations for cloud cover and suggested a new empirical formulation based on the Air Force Global Weather Central 3D analysis of cloud cover; according to his analysis, a clear-cut RH_c may not be justified. Models which assume this highly parameterized relationship tend to underestimate cloud coverage at $RH < RH_c$, especially in the mid-troposphere (850–600 mb), where the largest cloud amounts have been observed even at relative humidities below 60–80% [20]. The model also tends to overestimate the cloud cover at $RH > 90\%$, a condition which generally occurs in the PBL. Additionally, the MM5V3 cannot distinguish different types of clouds, nor can it model the small-scale variability within the clouds.

The middle and low cloud fractions at 1800 UTC on July 17, simulated by the BLPBL and GSPBL, are shown in Figures 3a–d. The BLPBL generated large areas having mid-level clouds (800–450 mb; see Figure 3a), while the GSPBL

generated mid-level clouds only in isolated locations (see Figure 3b). This may be due to differences in the vertical mixing of water vapor. If a moist layer reaches 800 mb, it will significantly increase mid-level clouds, as the mid-level cloud cover is determined by the maximum RH between 800–450 mb. Figure 3a, then, suggests that the BLPBL scheme mixes water vapor over a much deeper layer than does the GSPBL (as illustrated in Figures 4c and 4d). Figures 3c and 3d show that both PBL schemes generated a large amount of low clouds. Overestimation of low clouds may lead to an inaccurate estimation of surface temperatures and PBL parameters.

A rigorous comparison between the observed and predicted cloud cover, while valuable in its own right, is beyond the scope of this paper. First of all, there are no measurements of the vertical structure of the observed clouds available to us during the time of this analysis; hence, one would need to make gross assumptions about how to combine the predicted high, mid-level, and low cloud cover for comparison to an observed column amount from a satellite image. Also, as previously stated, clouds are highly parameterized in MM5, with a tendency to underpredict cloud cover in the mid-troposphere and overpredict cloud cover in the PBL. Further model development on cloud-radiation physics is, therefore, greatly needed in the future.

6. PBL Structure and Evolution

Even though the BLPBL and GSPBL predicted very similar results in terms of sea level pressure, near-surface temperatures, and winds, significant differences were found in the diagnostic fields – including PBL height – during July 15–20, 1999. All of the differences in the simulated PBL structure and evolution are attributable to the differences in vertical mixing mechanisms between the BLPBL and GSPBL, since the model settings are otherwise identical.

6.1. VERTICAL STRUCTURE AND PBL HEIGHT

Figures 4a, 4c, 4e, and 4g (left panels in Figure 4) display, respectively, θ_v, specific humidity (q_v), RH and vertical circulation fields along the New Jersey cross-section (see Figure 1), with the land-ocean interface about halfway along the cross-section, at 1800 UTC on July 17, predicted by the BLPBL scheme. The same fields are shown for the GSPBL scheme in Figures 4b, 4d, 4f, and 4h (right panels in Figure 4). Significant differences are evident in the PBL thermal structure; the BLPBL predicted much higher and well-mixed θ_v and q_v fields over land reaching about 800 MB, or 50–100 mb higher than that predicted by the GSPBL. The BLPBL predicts an RH of 100% at 800 mb, while the GSPBL-predicted maximum RH is only about 60–80% at 800 mb. This explains the significant differences in the diagnosed mid-level cloud cover shown in Figures 3a and 3b. The non-local vertical mixing mechanism in the BLPBL seems to be more efficient in generating a deeper and well-mixed moist layer in the lower atmosphere than the GSPBL. Both schemes,

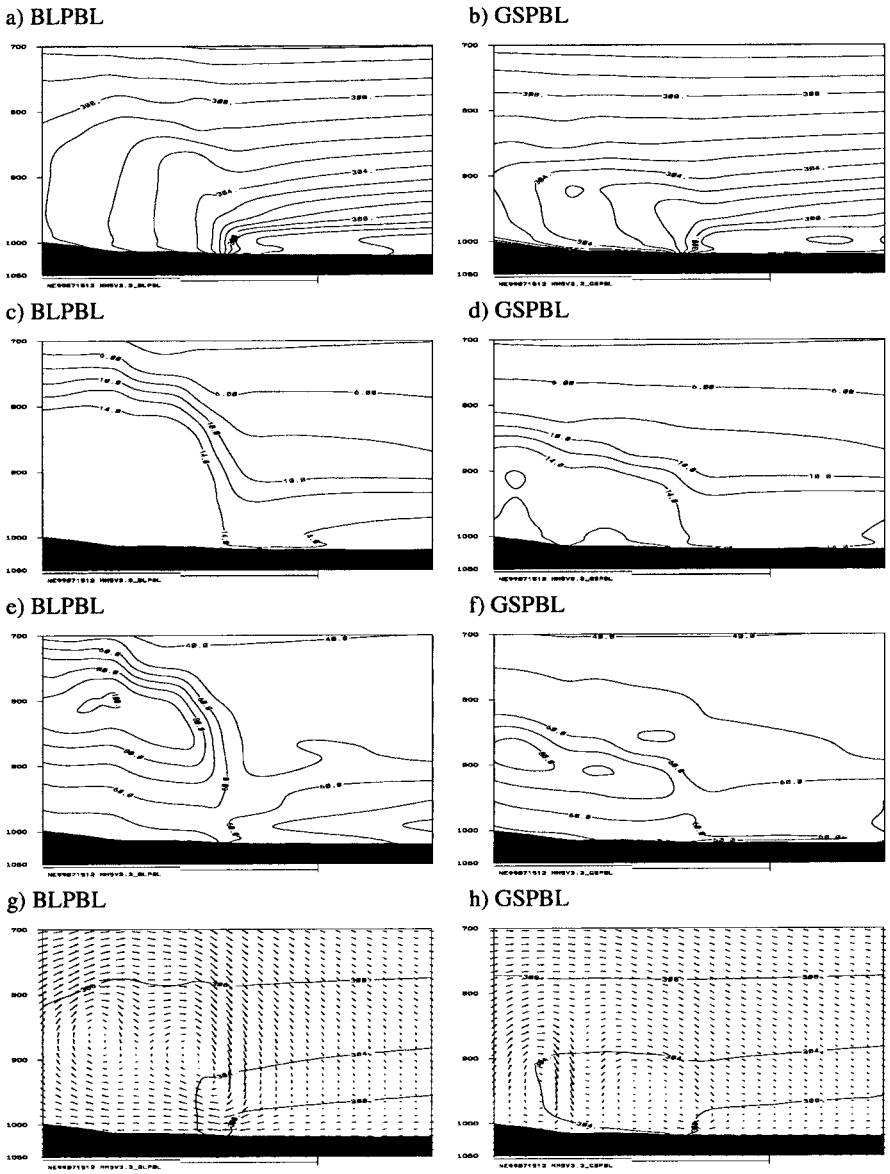

Figure 4. Predicted fields along the New Jersey cross-section at 2000 UTC on July 17: (a) BLPBL, virtual potential temperature (θ_v); (b) GSPBL, θ_v; (c) BLPBL, specific humidity (q_v); (d) GSPBL, q_v; (e) BLPBL, relative humidity (RH); (f) GSPBL, RH; (g) BLPBL, winds (with θ_v overlapped); and (h) GSPBL, winds (with θ_v overlapped). The lines under each panel are about 100 km.

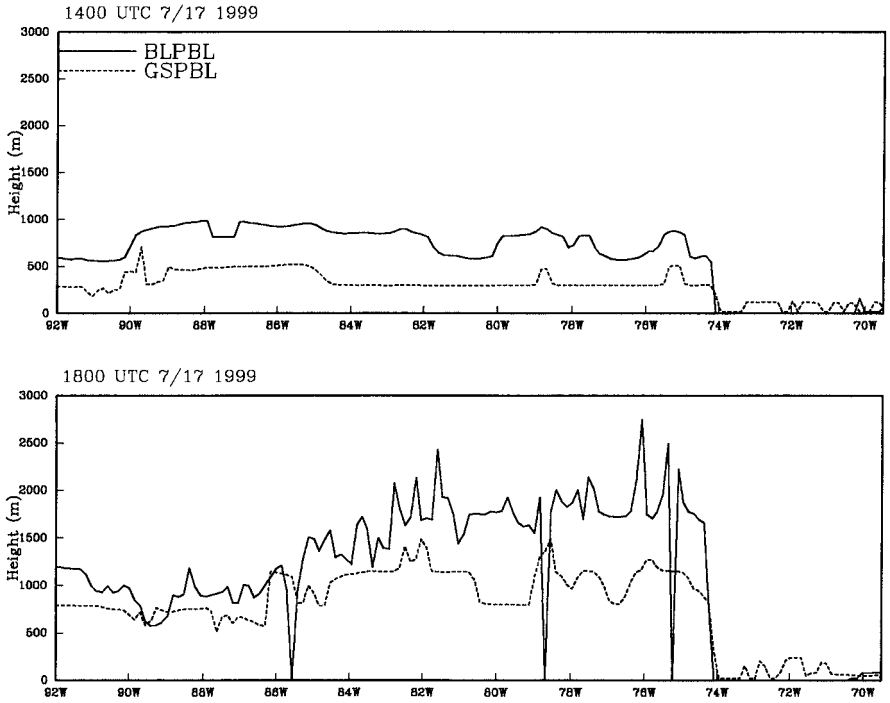

Figure 5. Simulated PBL heights along the west-to-east cross-section shown in Figure 1, at 1400 UTC (top panel) and 1800 UTC (bottom panel) on July 17.

however, predicted transitions from a deep mixing layer over land to a shallow layer over the Atlantic Ocean. However, the BLPBL generated a stronger sea breeze circulation than the GSPBL, as shown in Figures 4g and 4h, respectively. The larger sea breeze circulation predicted by the BLPBL is due to the more efficient vertical transport of heat flux over land, which creates a larger land-sea contrast above the surface.

Figure 5 shows the PBL heights predicted by the two PBL schemes at 1400 UTC (top panel) and 1800 UTC (bottom panel) along the west-to-east cross-section through the 12-km domain, shown in Figure 1. It is clear that the PBL height diagnosed by the GSPBL scheme is systematically lower than that of the BLPBL scheme both during the morning and afternoon hours. The differences over land are about 300–500 m at 1400 UTC, and greater than 1000 m at 1800 UTC, east of about 81° W. The overall difference in PBL heights between the two models is about 50%. Also with the BLPBL scheme, the stability regime can change dramatically, as noted in the PBL collapse near 85.5° W, 78.8° W, and 75.2° W. This artificial collapse will be discussed in a later section. The reason for the substantially lower PBL height diagnosed by the GSPBL is that the predicted turbulence (TKE) cannot support a higher mixing layer. It is clear, then, that we need to determine whether convection or diffusion is better able to generate a more 'realistic' mixed layer.

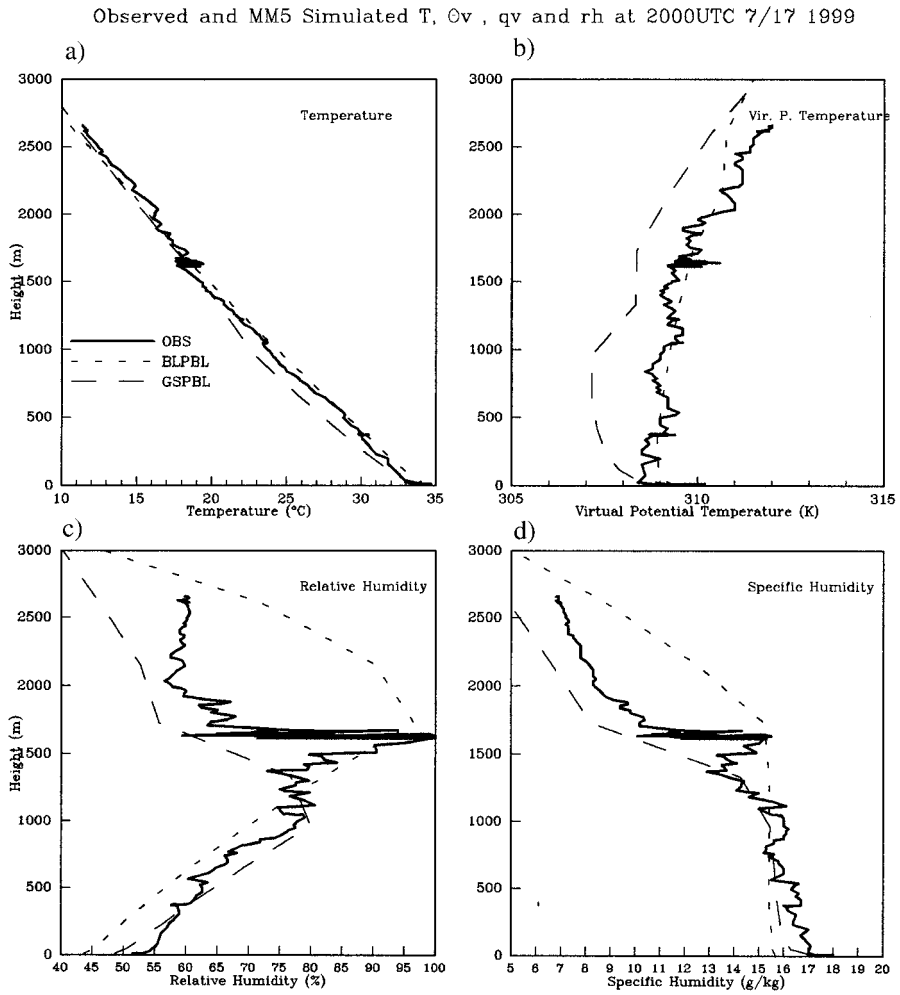

Figure 6. Aircraft spiral measurements of (a) T_v; (b) θ_v; (c) RH; and (d) q_v over PNE around 2000 UTC on July 17, and the corresponding BLPBL and GSPBL simulations.

Figures 6a–d show the profiles of virtual temperature (T_v), θ_v, RH, and q_v obtained from an aircraft spiral, and from MM5V3 at the grid cell that encompasses PNE around 2000 UTC on July 17. Several shallow inversions occurred between 1.7–2.2 km. A simple way to estimate the PBL height from the observations is to draw a vertical line from θ_v in the surface layer and find the intersection in the mixed-layer. The aircraft observations suggest that the mixed-layer height ranged from about 1.7 to 2 km. Although not shown here, profiles of O_3 also suggest that the height of the PBL is near 2 km, but the estimates of PBL height will be slightly different when using profiles of different scalars. On the other hand, the model-diagnosed PBL heights are 2.2 km by the BLPBL, and 1.1 km by the GSPBL. It is also obvious that even though the GSPBL predicted slightly higher temperature

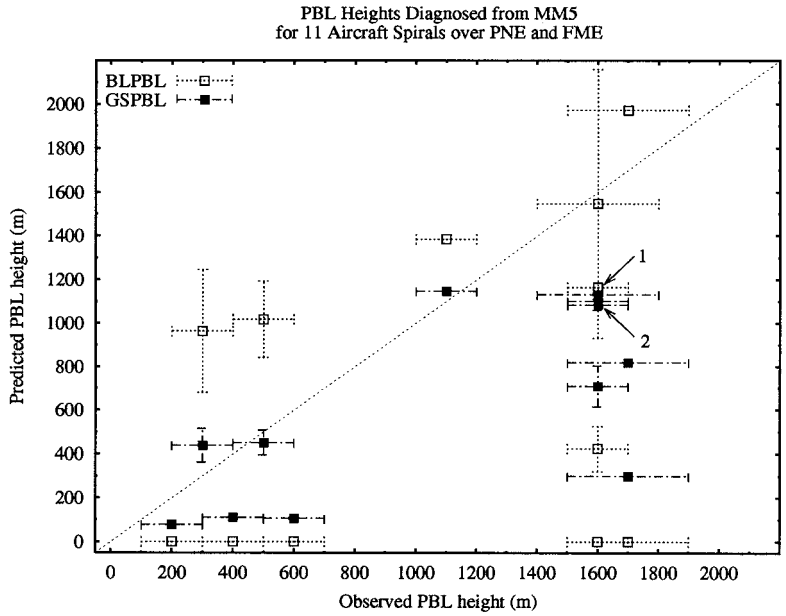

Figure 7. PBL heights predicted in the two original model simulations, compared with aircraft observations for 11 spirals over PNE and FME from July 17–19, 1999. The 1:1 line (dotted) is also shown. The error in observed PBL estimates, due to uncertainties in the height estimates and profiles of different scalars, is about 100–200 m. If a spiral nearly coincided with the top of an hour, only one PBL height is shown; otherwise, the range from one hour to the next is shown. The data points labeled '1' (BLPBL) and '2' (GSPBL) correspond to the model predictions shown in Figure 6.

fields at the surface, the GSPBL predicted lower T and θ_v ($\sim$2 °C) throughout the rest of the mixed-layer. In fact, although not shown here, a 1–2 °C bias was observed at 2000 UTC along most of west-to-east cross-section, from about 86° W to the coastline (74° W). At the same time, the BLPBL overpredicted q_v and RH above the well-mixed layer ($>$1.7 km). A significant feature in the observations is the sharp gradient in q_v and RH at the top of mixed layer, but the model does not have sufficient vertical resolution ($\sim$400 m) to resolve this feature near 1.7 km (see Table I).

While Figures 6a–d compare the predicted and observed profiles at one time, Figure 7 compares the estimated PBL heights during 11 aircraft spirals from July 17–19 over PNE and FME. In Figure 7, when a spiral nearly corresponds to the top of an hour, the model-predicted PBL is shown; when a spiral occurred during an hour, the range in model-predicted PBL height is shown. In all cases, the observed PBL height has an uncertainty of about $\pm$100–200 m, since the height of the spiral is estimated from the ambient pressure and assumes a standard atmosphere, and because profiles of different scalar quantities can suggest slightly different PBL heights. Except for five of the nighttime profiles (where the BLPBL scheme sets the PBL height to the lowest model level), the BLPBL may overestimate the PBL

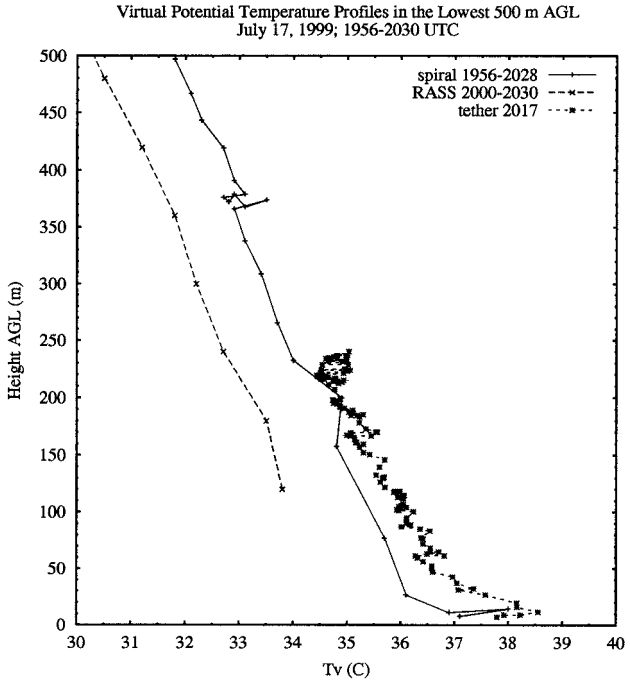

Figure 8. Aircraft spiral, tethered balloon, and RASS profiler measurements of T_v around 2000 UTC on July 17.

height, while in general the GSPBL scheme tends to predict lower PBL heights. Given so few profiles during this period, this should be viewed as only a tentative assessment of the model's ability to reproduce the observed PBL heights.

Uncertainties exist not only in model simulations, but also among the different measurements. Figure 8 displays a typical T_v profile on July 17, suggesting that 1–2 °C differences between the aircraft, tethered balloon, and RASS profiles are possible. As summarized by Angevine *et al.* [21], T_v measured by RASS is only accurate to about 0.5 °C. Also, when the authors compared RASS to tower-based measurements, they found the mean bias and standard deviation of the biases to be about 1 °C. These measurement uncertainties need to be taken into consideration when comparing model predictions with observations, as in Figures 6a–d and 7.

6.2. PBL EVOLUTION

Figure 9 shows the time series of model-predicted PBL heights at the Baxter site from July 15–20. The GSPBL diagnosed the maximum PBL height to be about 1200 m during the first four days, about 800 m lower than that predicted by the BLPBL. In addition to the 30–40% difference in the PBL height, Figure 9 shows that the GSPBL predicted a slower growth rate for the mixing layer and a PBL collapse time about 1–2 h later than the BLPBL. This is due to the generation and

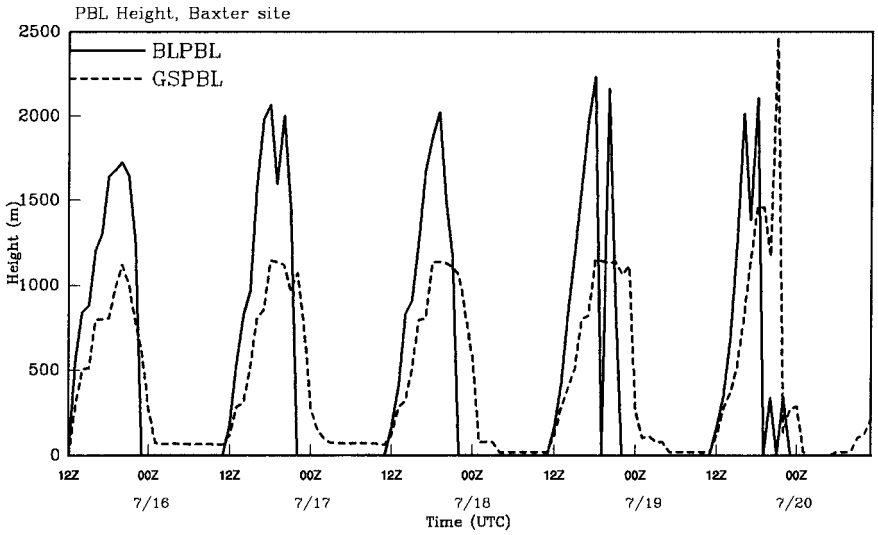

Figure 9. Time series of simulated PBL height by the BLPBL and GSPBL schemes at the Baxter site, from July 15–20. All 5-day time series and time-height cross-sections start at 1200 UTC on July 15 and end at 1100 UTC on July 20.

dissipation of TKE, and the fact that vertical mixing by layer-to-layer diffusion is slower than direct non-local mixing by convection. The thermal stability regimes of the PBL can change rapidly in the BLPBL, which determine when direct mixing takes place. Berman *et al.* [22] showed that the maximum mixing height at New Brunswick, NJ during the July 13–15, 1995 episode ranged from about 1400–2200 m, using meteorological fields from a similar MM5 simulation (with the BLPBL) scheme and from two sets of independent observations – sonde-based T_v, and profiler-based refractive index structure parameter (C_n^2) measurements. The authors determined that the BLPBL was able to simulate both the morning growth rate and the height of the PBL quite well during this episode. Using a different set of independent observations for model comparison, and considering a different synoptic situation (mid-July 1999), our results also suggest that the mixing processes of the BLPBL are able to simulate the behavior of the convective PBL rather well.

On the timescales of vertical mixing processes (<1 h; discussed in the following section), water vapor can be thought of as an inert PBL tracer (without significant evaporation or formation from clouds, fog, or rain). Thus, its vertical distribution can be used as an indicator of vertical mixing in the PBL. Figures 10a and 10b show the simulated time-height cross-section of q_v during July 15–20 at the Baxter site from the BLPBL and GSPBL schemes, respectively. The 14 g kg^{-1} isoline reached 1.5 km during the daylight hours on July 17 in the BLPBL simulation, while the GSPBL predicted a more stratified q_v field with significant vertical gradients varying from 17 g kg^{-1} to 12 g kg^{-1} below 1.5 km. It is clear that the non-local vertical

mixing mechanism used in the BLPBL is more efficient than the eddy-diffusion mechanism of the GSPBL in generating a deep, well-mixed layer in the PBL. This systematic difference in the structure and time evolution of the PBL appeared on each day from July 16–19.

Aircraft profiles of q_v over PNE during the afternoon hours of July 17–19 (Figure 11) suggest that water vapor is well-mixed below about 1.5 km. That is, the vertical gradients in q_v are generally small within the PBL. Limited lidar data on July 15 and 16 (not shown) also suggest that below about 1–1.5 km, water vapor profiles are fairly uniform. Hence, although the models do not have adequate vertical resolution to capture the small-scale features in the q_v profile, nor can MM5V3 necessarily reproduce the day-to-day variations in the absolute magnitude of q_v, it appears that the non-local vertical mixing in the BLPBL scheme more closely resembles observed profiles of uniform q_v below 1.5 km than does the eddy-diffusion GSPBL scheme.

6.3. IMPLICATIONS OF LARGE-EDDY SIMULATION (LES)

Even though profiler/lidar observations reveal valuable information on the time-height evolution of PBL, such fixed-location measurements cannot describe the three-dimensional turbulence structure. To identify the small-scale but efficient dynamical processes responsible for vertical mixing, large-eddy simulation (LES) has been developed. For example, Moeng [23] used a spectral LES model (5 km $\times$ 5 km horizontal domain, 2 km vertical extent) to generate convective updrafts and downdrafts with horizontal and vertical scales of about 1 km. After about 24 min (3 characteristic turnover times) a uniform $\theta-$field is formed below 1 km [24, 25].

As noted above, the BLPBL is more efficient in vertical mixing than the GSPBL in terms of the growth rate of PBL height (Figure 9), as well as vertical mixing of water vapor (Figures 10a and 10b). Note that for the BLPBL (Figure 10a), the local time rate of change in q_v ($\partial q_v/\partial t$) is rather large around 1200 UTC each day; that is, the isolines of q_v are nearly vertical. The GSPBL (Figure 10b), on the other hand, predicts that q_v varies more slowly in time. In Moeng's LES study [23], complete vertical mixing of the q_v profile can be achieved within 24 min, implying a $\sim$0.5 h timescale for vertical mixing in the convective PBL. Since the BLPBL parameterizes large eddy mixing by using non-local closure, it should be more representative of the LES-simulated convection cells than the GSPBL scheme. Pleim [26] compared an eddy diffusion scheme with an asymmetric convective scheme (non-local exchange for updrafts and local exchange for downdrafts) in a chemical model (RADM), also reporting faster upward transport of ground-level emissions and pollutants by the non-local mixing as compared to the eddy diffusion scheme. Zhang and Rao [27], incorporating both local and non-local vertical mixing in a photochemical model (MAQSIP), also showed differences in O_3 production were greatest in the early morning. Around 0900 EST, the non-local scheme produced an O_3 tendency about 4–5 ppb h^{-1} larger than the local scheme; during the afternoon

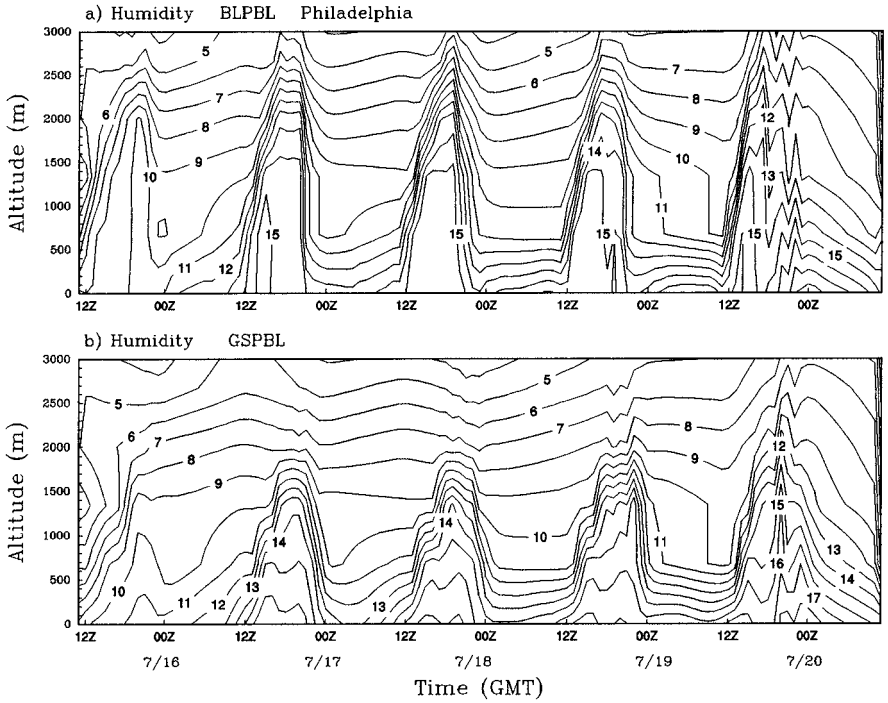

Figure 10. Time-height cross-sections of q_v at the Baxter site from July 15–20: (a) BLPBL; and (b) GSPBL.

hours, the non-local scheme predicted a higher mixing layer and more dilution [27].

7. Low-Level Jets (LLJs)

Low-level jets are salient features within the PBL [28–30]. They are important agents for the transport of water vapor and pollutants within the lower atmosphere. It is difficult to detect and predict LLJs operationally, since they are shallow in both the vertical (200–600 m in depth) and horizontal (at meso-β) scales. While LLJs may persist a few days over the ocean as part of large synoptic systems, over land they are subject to diurnal variation and last only a few to 12 h. Operational weather observation networks, having spatial resolution of about 400 km and relying on twice-per-day soundings, are inadequate for studying the LLJs. Therefore, the integration of continuous remote sensing observations and numerical models becomes necessary to form a more complete understanding of the evolution and dynamics of LLJs.

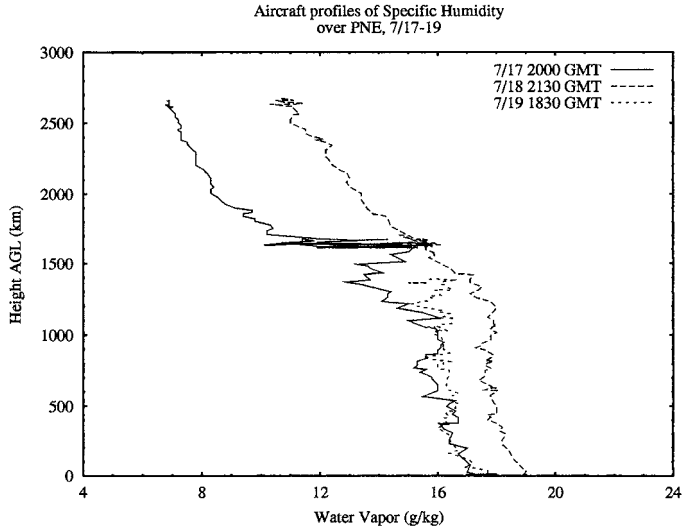

Figure 11. Selected afternoon aircraft profiles of q_v over PNE on July 17–19.

7.1. CHARACTERISTICS OF OBSERVED LLJS

Figures 12a–c show the time-height cross-sections of the horizontal winds measured by the RASS profiler at the Baxter site, from July 16–18, respectively. Under stable synoptic conditions, the LLJ appeared each night. The timing of onset is not always the same from night to night, since LLJs are generated dynamically, rather than by diurnal thermal forcing. During the daytime, LLJs are weakened by vertical mixing processes over land. On each day, the wind speed began to increase after sunset (about 0000 UTC) and reached a maximum at 0700, 0400 and 0800 UTC on July 16, 17, and 18, respectively. The LLJs were maintained well into the morning hours on July 16 and 18, but to a lesser degree on July 17.

Based on the conventional definition of an LLJ – that the maximum wind speed at the jet core should be at least 3 m s^{-1} larger than above and below the core – the LLJs formed around 300–700 m above ground on each of the three days. Note that in this study, the closest model levels are set at 411 m and 654 m; higher vertical resolution ($\sim$100 m) is needed in order to properly simulate the vertical structure of the LLJs. The maximum wind speed sustained for more than 1 h was 13 m s^{-1}, 14 m s^{-1}, and 12 m s^{-1} on July 16, 17, and 18, respectively (see Figures 12a–c). The jet core wind speeds above 10 m s^{-1} can persist up to 12 h. The wind directions generally rotated from southwesterly near the surface to more westerly aloft, starting around 0000 UTC.

7.2. LLJS SIMULATED BY MM5V3

Figures 13a–e show the observed and MM5V3-simulated time-height cross-sections of wind speed at the Baxter site from July 15 (1200 UTC) to 20 (1100 UTC).

Figure 13a shows the RASS observations, with only the 6 and 10 m s^{-1} contours shown for clarity. It is obvious that in both the BLPBL (Figure 13b) and GSPBL (Figure 13c), the wind speeds were underpredicted by about 4–6 m s^{-1}. In the vertical, the simulated heights of jet cores are about 400–600 m. Since the model levels nearest to the jet core are located at 411 m and 654 m, it is difficult to simulate the height of the jet core accurately. Also, the model cannot reproduce the sharp gradients near 400 m as indicated by the observations, which may also be caused by underestimation of nighttime turbulence below 400 m. In addition to the original simulations, the results of the modified LLJ experiments, shown in Figures 13d and 13e, will be described later.

In addition to the underprediction of wind speeds, the models cannot reproduce the timing of onset of the LLJ either. Both the BLPBL- and GSPBL-simulated LLJs reached maximum wind speeds at 0000 UTC, but could not sustain the jets for more than 6 h. As indicated by the observations (Figures 12a–c), LLJs reached maximum wind speeds around midnight and maintained them well into the next morning on July 16 and 18. One reason that MM5V3 could not reproduce these features is that in the original model configuration, FDDA was applied in the lower atmosphere after the PBL collapse. Also note in Figure 13b that the BLPBL was able to simulate a more vertically uniform pattern, and was able to mix momentum down to near the surface during jet intensification. Wind speeds in the BLPBL simulations are sometimes greater than 6 m s^{-1} below 200–400 m, which is not in agreement with the observations. In contrast, the GSPBL developed a diamond-shaped pattern, suggesting that, again, vertical mixing is faster in the BLPBL simulations. Because of FDDA, both sets of simulated wind fields reach a maximum at 0000 UTC, which does not coincide with the observations.

Figures 14a–e shows the same information as in Figures 13a–e for wind directions. The west-southwesterly flow contour is emphasized for clarity. The dominant westerly flow, the turning with height, and time evolution are fairly well-simulated for the first three days by both PBL schemes. Wind direction, turning from southwesterly to westerly, is more clearly shown in Figure 15a near the simulated height of jet core (654 m). The simulated pattern of evolution compares fairly well, at least qualitatively, with the observations during the nighttime hours, when wind speeds are largest. Larger discrepancies in wind direction occur during the daytime hours, when horizontal wind speeds are generally lower and convective mixing is vigorous within the PBL. Note that such discrepancies in wind direction, could, in turn, cause pollutants trapped aloft in the residual layer to be transported along different directions.

The original MM5V3 simulations did not reproduce the LLJ well in terms of timing, strength, and vertical structure. The main reason is that the FDDA nudging fields, based on twice-per-day soundings at 0000 and 1200 UTC, do not have sufficient temporal resolution to delineate the LLJ evolution. After the PBL collapse during nighttime hours, the nudging tends to dampen the LLJ features and shift the LLJ onset closer to one of the sounding times (which has higher wind speeds).

In the next section, we describe the modified simulations, in which the model was able to better simulate the LLJ structure by limiting the nudging even further.

7.3. IMPROVING THE SIMULATION OF THE LLJS

As noted in Section 6.1, the BLPBL-predicted PBL heights are very sensitive to surface stability, and sudden changes in surface stability may lead to abrupt jumps in the diagnosed PBL height. Holtslag and co-authors [31] suggested that the PBL height can be determined at the level at which the bulk Richardson number exceeded a critical value of 0.25. The group at MCNC (see *http://envpro.ncsc.org/SMRAQ/meteorology/reports*) showed that this new method [31] allowed for a more gradual collapse after sunset, and did not artificially set the nighttime PBL height to the lowest model level. However, the MODELS-3 system applies a similar PBL height method (see Ku *et al.* [4]), and it is possible that the methods proposed by Holtslag and co-authors tend to overpredict PBL heights by ∼500–1000 m [32].

In order to better simulate the daytime PBL and the nocturnal LLJ structure, two developments have been introduced to the original MM5V3. First, in order to eliminate the collapse of PBL height at isolated locations during the daytime by the BLPBL scheme (see Figure 5), the convective energy computation is applied to all PBL regimes, instead of allowing the artificial PBL collapse in the stable surface layer ($Ri_{sfc} > 0$). In the original BLPBL scheme, the stable regimes were classified according to surface parameters alone. There are certainly times when a stable surface layer is indicative of a stable PBL as a whole. However, this classification may not reflect the potential of the PBL as a whole to support convection. Surface stability alone is not sufficient to characterize the potential for convection over the entire PBL, such as when there is positive convective energy above a stable surface layer. With this modification, the PBL heights over land are more reasonably diagnosed, and the sudden collapse of the PBL in isolated areas is eliminated.

The second modification, mentioned previously, is the exclusion of FDDA from the lower atmosphere. In this modification, FDDA is only applied to the atmosphere above the diagnosed PBL height or the lowest 8 model layers (∼1.3 km), whichever is higher, since the jet core occurs near 400–700 m and the effects of the jet extend to about 1 km. Hence, the lower atmosphere is always free from nudging, both during the daytime and nighttime. This approach is similar to the work by Shafran *et al.* [2], who limited FDDA to above 1.5 km, leading to the improved simulation of the low-level wind fields, and possibly limiting the daytime development of the PBL.

With the above modifications to MM5V3, the new experiments, denoted as the MBLPBL and MGSPBL simulations, were carried out for same period. Figures 13d and 13e show the wind speeds, and Figures 14d and 14e show the wind directions simulated by the MBLPBL and MGSPBL, respectively. Note that in the modified simulations, the maximum wind speeds in the vicinity of the jet during the nights of July 16–18 increased to about 10 m s^{-1}. The improvement in the

strength of the LLJs is substantial; while the original MM5V3 predicted jet core maxima which are about 50% as high as the observations, the modified MM5V3 is able to predict jet core maxima that are about 75–90% of the observed wind speeds. The modified PBL simulations, therefore, have better simulated the LLJ strength, especially on July 16. Although the modifications led to higher wind speeds, the model was still not able to reproduce the sharp vertical gradients near 400 m since the vertical resolution was kept the same, and because of the weak nocturnal turbulence. The BLPBL and MBLPBL simulations both predicted winds speeds higher than observed extending to the surface, while the MGSPBL scheme predicted large wind speeds (>6 m s^{-1}) only above about 100 m.

The most significant improvement occurs in the timing of the LLJs. Because the modified simulations are free from FDDA below 1.3 km, the low-level wind fields are controlled by the intrinsic dynamics. The simulated LLJs now reach their maxima at 0600, 0300 and 0600 UTC in the MBLPBL experiment, and at 0700, 0100 and 0800 UTC in the MGSPBL experiment on July 16–18, respectively. These timings of occurrence of the maximum LLJs are closer to the observations than the 0000 UTC predicted by the original experiments (Figures 13b and c).

The time-height cross-sections of the modified wind directions are displayed in Figures 14d and 14e, while the time series of the wind direction and speed at 654 m are shown in Figures 15a and 15b. During the daytime hours, southwesterly flows were predicted by both modified simulations, extending to about 1 km; however, westerly flow near the surface on July 17 was not captured well by the modified simulations. During the morning hours, westerly flow dominated the observed wind near 654 m. The wind direction suddenly changed to southwesterly between 1800–2100 UTC, due to upward mixing of momentum. During the nighttime, the wind direction slowly changed to westerly with increasing wind speeds, reflecting a decoupling of the LLJ and the surface layer. This diurnal pattern occurred on each of the first four days before a cold front arrived on the last day. All simulations were generally able to model the diurnal cycle, but tended to lead observations by a few hours during the daytime as the wind direction changed from westerly to southwesterly. The best agreement between observations and simulations occurs during nighttime hours when the LLJs develop.

7.4. HORIZONTAL SCALE AND VERTICAL STRUCTURE OF THE LLJS

The model simulations can be used to examine the horizontal and vertical scales of the LLJs. Figures 16a–d show the simulated wind fields near the jet core height of 950 mb (654 m) at the time of peak wind speeds (0400 UTC) on July 17 (see Figure 12b). With FDDA, both the BLPBL and GSPBL generated similar wind fields; along the northeastern U.S. seaboard, the largest wind speeds (>10 m s^{-1}) occurred over Long Island and over the Atlantic Ocean off the coast of CT in both the BLPBL (Figure 16a) and GSPBL (Figure 16b) simulations. The situation is rather different in the MBLPBL (Figure 16c) and MGSPBL (Figure 16d) simula-

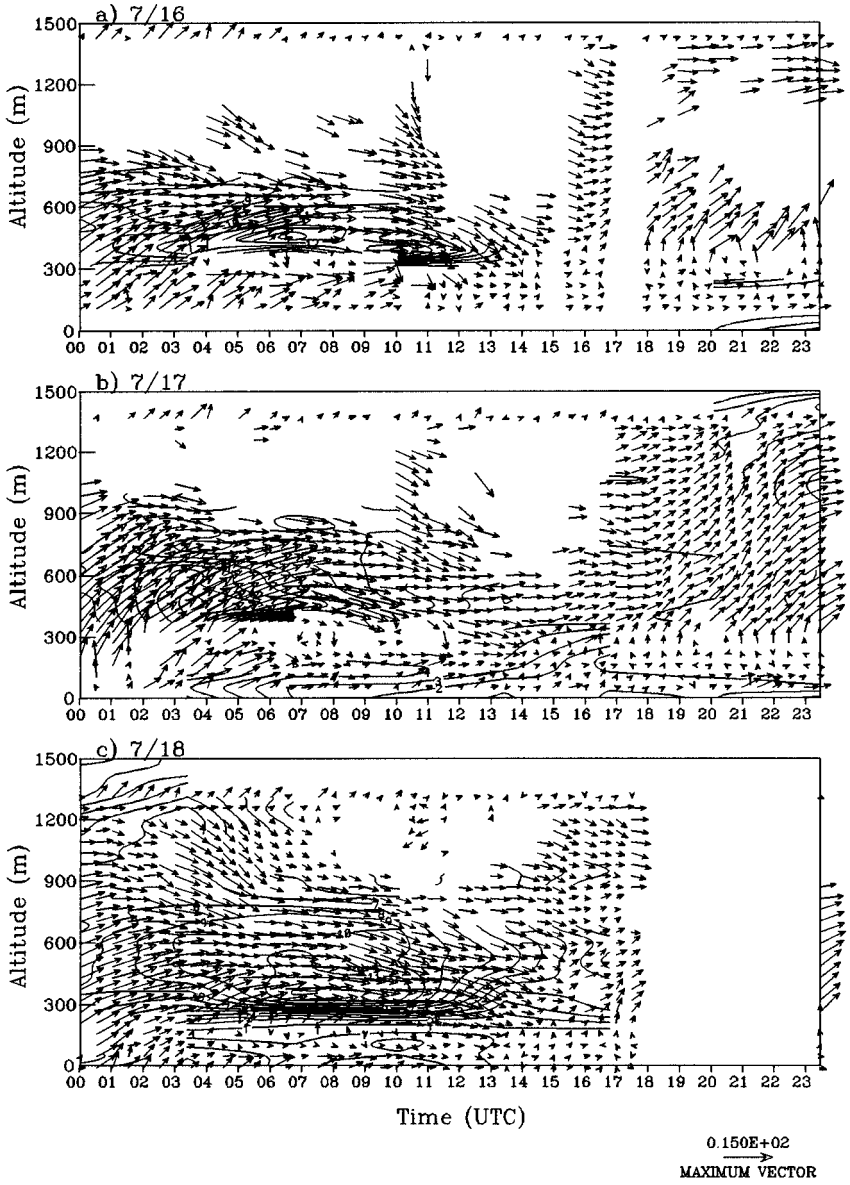

Figure 12. Hourly wind profiler observations at the Baxter site on (a) July 16; (b) July 17; and (c) July 18.

tions without FDDA. Horizontally, the simulated LLJs are more than 200 km wide. The MBLPBL simulation predicted maximum wind speeds near Boston, MA of 18 m s^{-1}, while the MGSPBL predicted a large region from NY to MA having wind speeds greater than 18 m s^{-1}, with a 20 m s^{-1} center over CT. Since the RASS profiler at Stow, MA did not detect such high wind speeds, it appears that

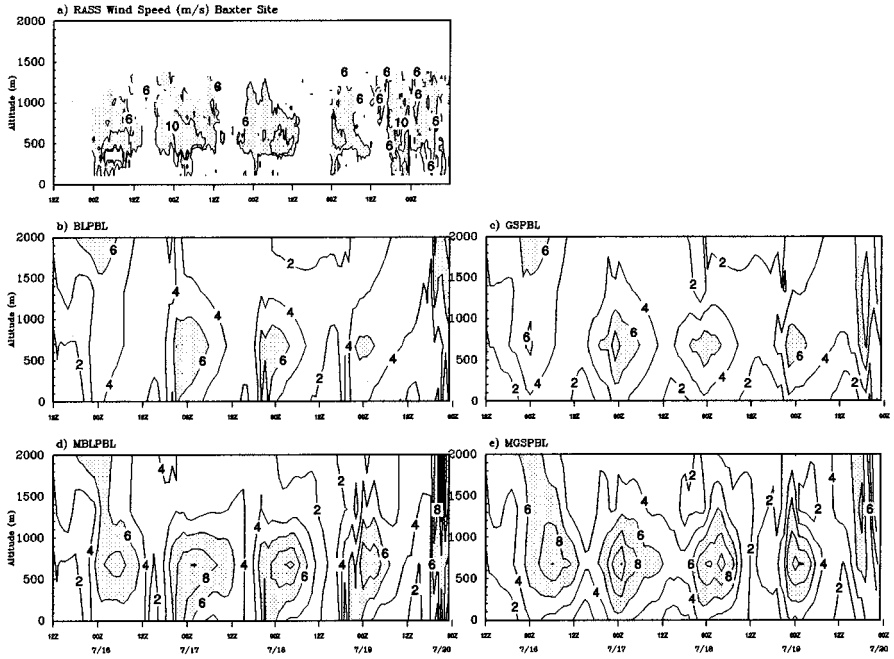

Figure 13. Time-height cross-sections of wind speed at the Baxter site from July 15–20: (a) wind profiler observations; (b) BLPBL; (c) GSPBL; (d) MBLPBL; and (e) MGSPBL.

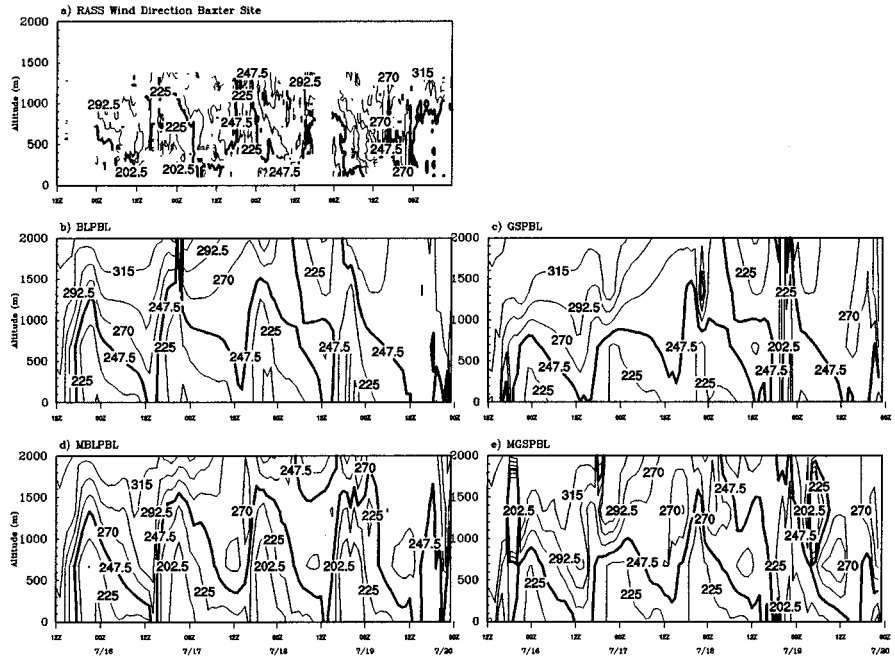

Figure 14. Same as Figures 13a–e, except for wind direction.

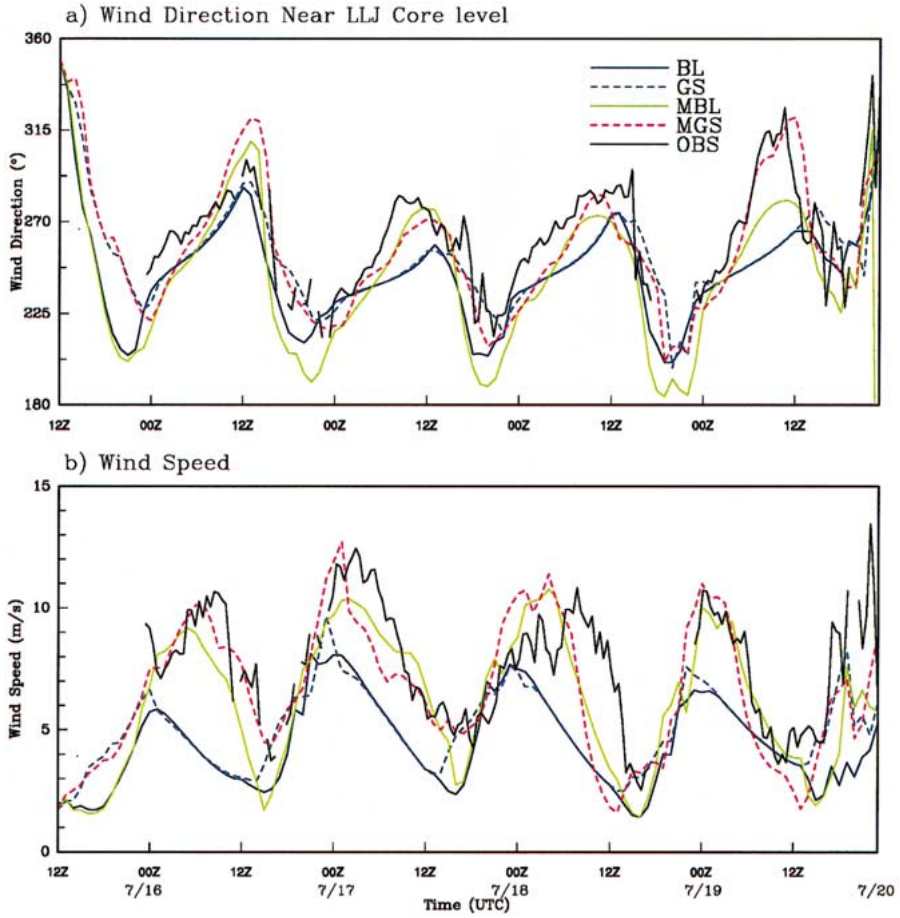

Figure 15. Time series of (a) wind direction and (b) wind speed at the Baxter site from July 15–19, at about 654 m (near the jet core), from the observations and the original and modified simulations.

the modified simulations actually overpredicted the jet intensity at this time. This may be due to the underestimation of nighttime turbulence.

The vertical structure of the LLJs along the New Jersey cross-section, simulated in the four experiments, is displayed in Figures 17a-d. The BLPBL (Figure 17a) and GSPBL (Figure 17b) predicted LLJs with wind speed below 10 m s^{-1}, which are weaker than the RASS observations. The simulated heights of the jet cores are too low, only at about 100–200 m by the GSPBL and 200–300 m by the BLPBL. The BLSPBL (Figure 17c) and GSLPBL (Figure 17d) predicted stronger LLJs on the order of 12–14 m s^{-1}, which are comparable to RASS observations at the Baxter site. The height of the jet core increases from about 200 m over the ocean to about 300 m over land in the MGSPBL, still too low compared to the 400–600 m level seen in the observations. The centers of the MBLPBL-simulated LLJs are

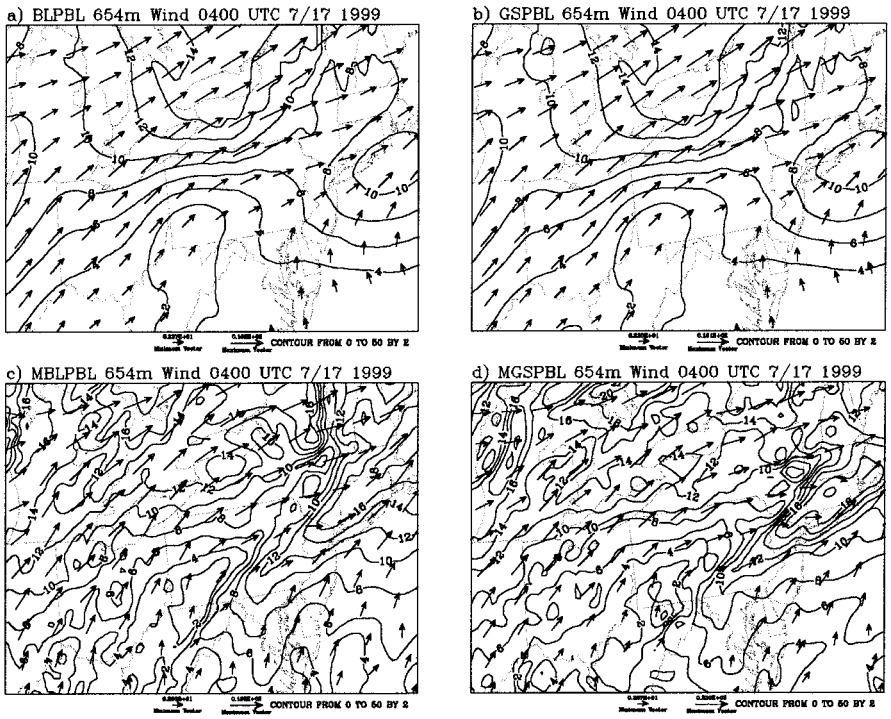

Figure 16. Simulated wind fields near the height of jet core (654 m) at 0400 UTC on July 17 by (a) BLPBL; (b) GSPBL; (c) MBLPBL; and (d) MGSPBL. Wind speed is shown in 2 m s^{-1} contour intervals.

located at 400 m over the ocean and about 600 m over land, in better agreement with the observations.

All of these model differences and uncertainties will affect air quality simulations in a non-linear fashion. This is important since, as noted before, pollutants trapped aloft in the residual layer are transported over large distances by the LLJs during the night. Differences in wind speed and direction will lead to different PBL ventilation and pollutant transport directions.

8. Statistical Evaluation of the Surface Level and Vertical Structure of PBL

8.1. SURFACE LEVEL

To summarize the overall performance of the MM5V3 simulations, we compared the hourly observed and predicted temperature, specific humidity, wind speed, and wind directions at the surface from the July 15–20 period. The statistics include the mean and standard deviation of the differences (defined as 'model prediction minus observation'), root mean square error (RMSE), index of agreement, systematic error, and unsystematic error [33]. The data were also separated by 'daytime' hours (1200–0000 UTC) and 'nighttime' hours (0000–1200 UTC).

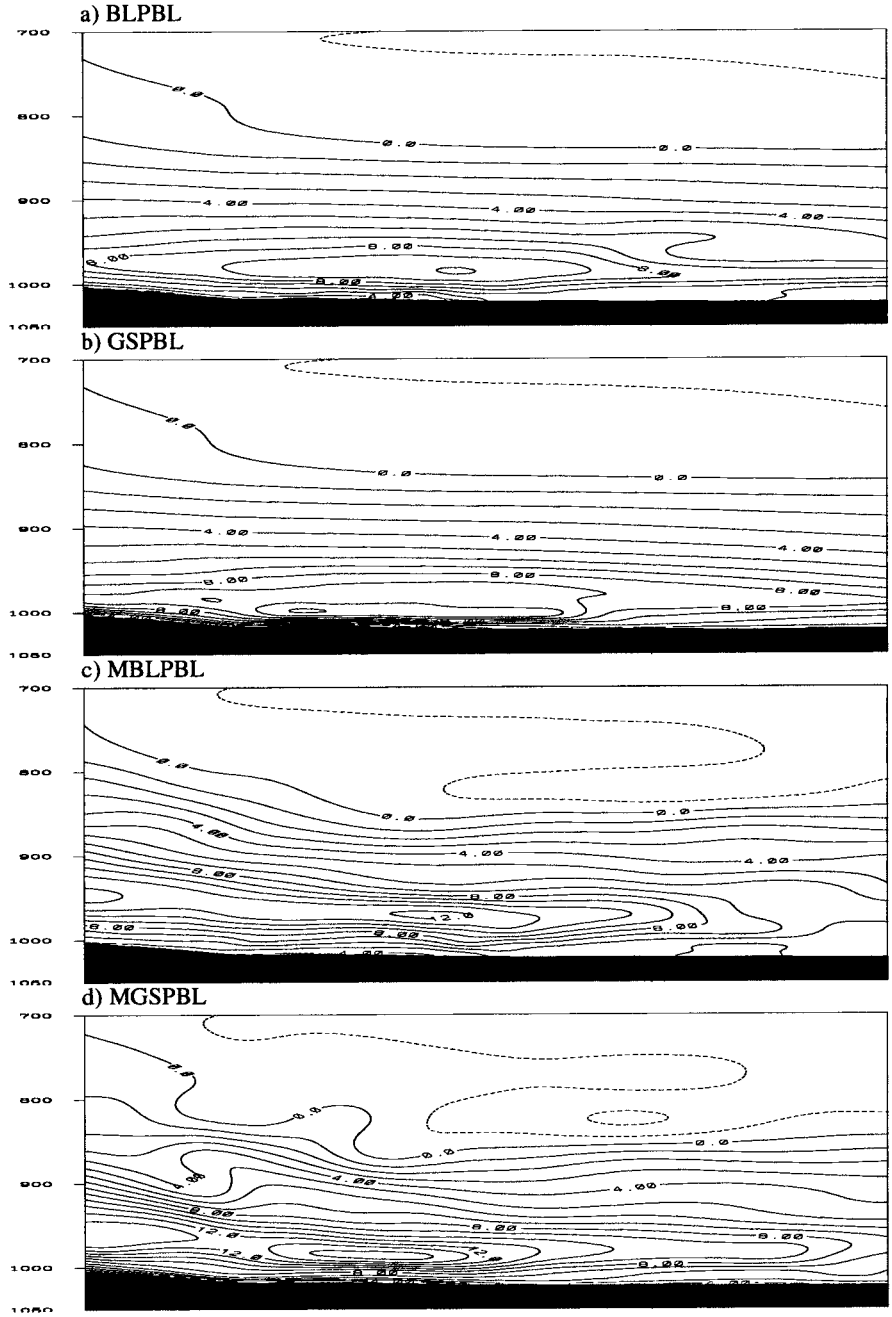

Figure 17. Simulated wind speeds along the New Jersey cross-section at 0400 UTC on July 17: (a) BLPBL; (b) GSPBL; (c) MBLPBL; and (d) MGSPBL. The Atlantic coastline is located near the middle of each panel.

Table III. Basic statistics for the hourly surface temperature observations and MM5V3 predictions during the July 15–20, 1999 period: (a) daytime hours, 1200–0000 UTC, and (b) nighttime hours, 0000–1200 UTC. The statistics shown are the mean difference, standard deviation (σ) of the difference, root mean square error (RMSE), index of agreement, systematic error, and unsystematic error. Differences are calculated as 'model prediction minus observation'.

Simulation	Mean difference (°C)	σ of difference (°C)	RMSE (°C)	Index of agreement (%)	Systematic error (%)	Unsystematic error (%)
(a) Daytime, 1200–0000 UTC						
BLPBL	−0.3	1.7	1.7	94	10	90
GSPBL	0.1	1.7	1.7	94	4	96
MBLPBL	−0.7	1.6	1.8	94	15	85
MGSPBL	−0.3	1.7	1.7	94	3	97
(b) Nighttime, 0000–1200 UTC						
BLPBL	0.9	1.5	1.7	91	30	70
GSPBL	1.0	1.5	1.8	91	31	69
MBLPBL	0.6	1.4	1.5	92	15	85
MGSPBL	0.8	1.4	1.6	92	26	74

The temperature statistics are shown in Table III. During the daytime, the BLPBL and modified PBL simulations on average have negative biases, while the GSPBL predicted a slight positive bias. In terms of the spread of the differences between the model and observations, the original and modified simulations had very similar standard deviations and RMSE values. In all cases, the unsystematic errors were substantially higher than the systematic errors. During the nighttime hours, where the effects of FDDA are pronounced, the biases were positive and larger than during the daytime. The systematic errors were also larger at nighttime than during the day.

Table IV shows the statistics for the specific humidity. The results are similar to temperature, in that the mean bias, standard deviation, and the RMSE were similar in all of the PBL simulations. The fact that the differences between the original and modified simulations for temperature and humidity are not substantial is not unexpected, since the modified FDDA scheme was used to improve the simulation of the vertical wind field structure (i.e., LLJs).

The situation with wind speed and direction is somewhat different (see Table V for wind speed and Table VI for wind direction). During the day, when surface wind speeds are low, there are substantial differences (∼55–60 deg) between the observations and predictions; the removal of FDDA greatly reduces these biases at

Table IV. Same as Table III, except for specific humidity.

Simulation	Mean difference ($g\ kg^{-1}$)	σ of difference ($g\ kg^{-1}$)	RMSE ($g\ kg^{-1}$)	Index of agreement (%)	Systematic error (%)	Unsystematic error (%)
(a) Daytime, 1200–0000 UTC						
BLPBL	0.8	1.4	1.6	82	25	75
GSPBL	2.0	1.5	2.5	70	65	35
MBLPBL	1.0	1.4	1.8	81	37	63
MGSPBL	1.9	1.5	2.4	71	64	36
(b) Nighttime, 0000–1200 UTC						
BLPBL	1.2	1.2	1.8	80	51	49
GSPBL	1.5	1.2	1.9	78	61	39
MBLPBL	1.5	1.2	1.9	78	59	41
MGSPBL	1.6	1.2	2.0	76	65	35

Table V. Same as Table III, except for wind speed.

Simulation	Mean difference ($m\ s^{-1}$)	σ of difference ($m\ s^{-1}$)	RMSE ($m\ s^{-1}$)	Index of agreement (%)	Systematic error (%)	Unsystematic error (%)
(a) Daytime, 1200–0000 UTC						
BLPBL	−3.3	3.0	4.4	51	55	45
GSPBL	−4.1	3.1	5.1	42	65	35
MBLPBL	−2.8	3.1	4.2	57	47	53
MGSPBL	−3.8	3.1	4.9	45	61	39
(b) Nighttime, 0000–1200 UTC						
BLPBL	−1.0	2.6	2.9	56	18	82
GSPBL	−1.3	2.7	3.0	53	23	88
MBLPBL	−0.5	2.7	2.7	63	4	96
MGSPBL	−1.1	2.7	2.9	57	18	82

Table VI. Same as Table III, except for wind direction. Negative wind direction biases indicate that on average, the model-predicted wind direction is rotated counterclockwise with respect to the observed wind direction.

Simulation	Mean difference (degrees)	σ of difference (degrees)	RMSE (degrees)	Index of agreement (%)	Systematic error (%)	Unsystematic error (%)
(a) Daytime, 1200–0000 UTC						
BLPBL	−59	149	161	50	12	88
GSPBL	−57	151	162	50	12	88
MBLPBL	−59	148	159	52	13	87
MGSPBL	−58	150	160	50	13	87
(b) Nighttime, 0000–1200 UTC						
BLPBL	−40	98	106	73	17	83
GSPBL	−41	97	105	72	18	82
MBLPBL	−38	100	107	74	19	81
MGSPBL	−40	99	108	73	19	81

night. Also, the unsystematic error at night is much larger than during the daytime. For wind direction, the day–night differences are also larger than the differences across the four simulations. This is not unexpected, since the effects of FDDA are largest at night, and frictional losses at the surface are the same in all simulations.

8.2. UPPER LEVELS

It is anticipated that the largest differences simulated by the two PBL schemes should occur in the vertical, since all simulations use common air-land interaction schemes and the same synoptic surface analyses in the FDDA fields. In this section, we attempt to quantify the differences between the observations and simulations by examining the mean and standard deviation of the biases, in the vertical. The observations are hourly-averaged RASS and wind profiles from July 15–19, 1999 from the Baxter site. All observations were averaged within the appropriate model layers (Table I) in order to compare with simulations; the observation levels were not interpolated to match the MM5 levels. The vertical extent is limited by the availability of observations. We did not include data from July 20 because of the passage of a cold front on that day. Bias statistics were generated for daytime (1200–0000 UTC) and nighttime (0000–1200 UTC) hours separately in order to identify the strengths and weaknesses of the schemes for each PBL regime. Although the biases above 1 km are displayed in the following figure, the limited

availability of observed data causes the largest biases to occur at this height; hence, we focus on comparisons below 1 km.

Figure 18 shows the observed mean profiles of daytime T_v and nighttime wind speed and direction, and the corresponding model biases at the Baxter site. The observations are shown on the left-most column. The respective biases of the BLPBL, GSPBL, MBLPBL, and MGSPBL are shown in columns 2–5, respectively. Note that the T_v observations are characterized as having an average daytime lapse rate of about 7 °C km^{-1}. The overall errors are small, with temperature biases less than 2 °C, except for the MGSPBL above 1 km. A systematic difference in the daytime bias profile occurs below 1 km: the BLPBL and MBLPBL are slightly positively biased (<1 °C), while the GSPBL and MGSPBL are negatively biased by about 1–2 °C. Again, this may be due to the fact that the BLPBL transports heat upward more efficiently. The negative bias of T_v during the daytime by the GSPBL and MGSPBL schemes implies that heat fluxes within the PBL have not been simulated well, or the strength of vertical mixing has been underestimated. Although not shown, the nighttime errors in T_v are generally small (<1–1.5 °C) below 1 km in all experiments.

The observed nighttime wind profile has a jet-like structure with a maximum of 8–9 m s^{-1} between 500–1000 m. Systematic positive biases below and negative biases above the lowest 2–3 levels (∼116 m) occurred in all experiments, suggesting an underestimation of dissipation at night. A negative bias near the jet core height means an underestimation of the strength of the LLJs. During the nighttime, both the BLPBL and GSPBL have a negative bias of 3 m s^{-1} near the jet core height. The modified schemes substantially improved the simulation of LLJ strength near the jet core, with a negative bias less than 1 m s^{-1}. At lower levels (below 411 m), a positive bias of 2–3 m s^{-1} also occurs in both the MBLPBL and MGSPBL simulations. This may be due to the sharp vertical gradient in observed wind speeds at about 400 m, and poor vertical resolution in the model, causing an underestimation of the dissipation below 400 m. Notice that the statistical error is much smaller than the day-to-day error caused by the underprediction of LLJs during the consecutive three nights of July 16–18, as shown in Figures 13a–e.

Wind direction below about 1 km is west-southwesterly (∼225 deg) during the nighttime, changing to westerly (∼270 deg) above. The wind direction errors are about 20 deg for the BLPBL simulation, and less than 20 deg for the GSPBL simulation during the daytime. The negative bias means that simulated wind directions are oriented more southerly. Larger biases appear in the MBLPBL and MGSPBL simulations above 1 km during the night, but the biases are rather small near the jet core height (654 m) in all experiments.

In summary, the average nighttime PBL at the Baxter site is characterized by a stable layer below 600 m, a weak jet-like wind speed maximum of about 8 m s^{-1}, with wind direction turning from southwesterly near the surface to westerly above about 1 km. The daytime PBL is characterized by a large lapse rate of T_v (∼7 °C km^{-1}) and more uniform wind directions. The original MM5V3 simulations un-

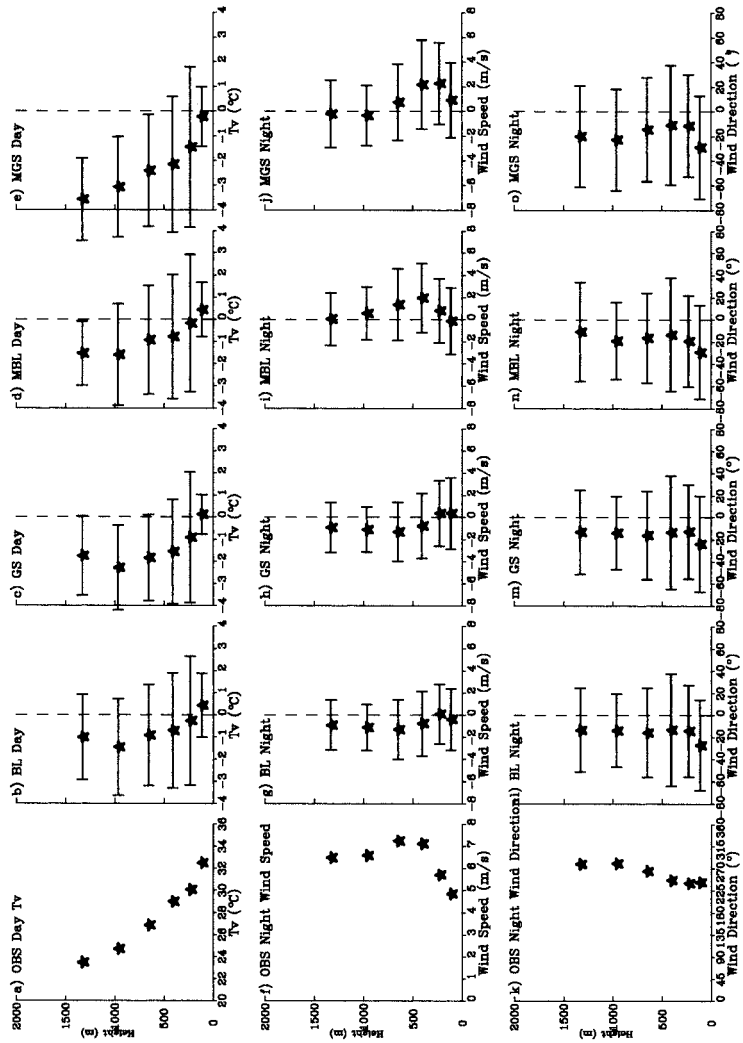

Figure 18. Statistics for observed daytime (1200–0000 UTC; top row) T_v and nighttime (0000–1200 UTC; bottom rows) winds, and respective hourly biases between model data and observations. The hourly data (leftmost column) cover the July 15–19 period, and include only the Baxter site profiler. The second column shows the mean and standard deviation of the biases between observations and the BLPBL simulation, for the same time periods. The third column shows the same for the GSPBL simulation. The fourth and fifth columns show the same for the MBLPBL and MGSPBL simulations, respectively. All biases are defined as 'model prediction minus observation'.

derestimated the strength of the nocturnal LLJ and the dissipation of energy below about 400 m, and tended to orient the wind direction more southerly than is indicated in the observations. Perhaps, the most important feature evident in these statistics is the fact that the biases in wind speed near the jet core were reduced in the modified simulations, although wind shear and, thus, turbulent mixing below about 400 m are still underpredicted.

In addition to errors within the modeling system, there are additional sources of uncertainty that can affect such a comparison. First is the uncertainty in the point-to-point comparison between observations and model outputs (or one model to another). Large errors can arise from relatively small temporal and spatial phase shifts, especially near regions with large gradients. It is not, therefore, a conclusive way to evaluate the model from a four-dimensional perspective. Another uncertainty related to this comparison stems from the differences between different measurement technologies (see Figure 8). In Figure 18, only the RASS data, which may not be as reliable above about 1 km, were used to calculate the bias statistics. By using different observational data as shown in Figure 8, one could expect a potential change in bias of T_v by $\sim$1 °C. We also found potential problems in the Stow, MA profiler data, including a jump in temperature of 8–10 °C from one hour to the next during the early afternoon hours, which would certainly have affected this evaluation had they been included.

9. Summary

In this study, we have performed parallel simulations using MM5V3 for the July 15–20, 1999 O_3/$PM_{2.5}$ episodic period, both with and without FDDA below the lowest 8 model levels, to examine the PBL evolution and structure, LLJ formation, and to generate the meteorological input for photochemical modeling. Using the surface and upper-air observations of meteorological variables, we were able to assess the four different simulations. The key findings of this study are as follows:

- With the original model settings, MM5V3 is able to simulate the characteristic structure and evolution of the PBL in terms of the diurnal variation of temperature, water vapor, and mixed-layer height. However, the original simulations could not simulate the timing or intensity of observed LLJs properly.
- The BLPBL simulations predict PBL heights that are closer to those observed by aircraft spirals. The GSPBL-diagnosed PBL height is generally too low. Comparisons with independent observations seem to support the non-local mixing mechanism in the convective PBL as opposed to the local eddy diffusion mechanism. The BLPBL scheme is more efficient in terms of vertical mixing.
- When FDDA is limited to above the lowest 8 model levels (i.e., above 1.3 km) in the modified BLPBL and GSPBL simulations, the model dynamics alone improve the simulation of the LLJs on July 16–18, although the model still

cannot predict the intensity of the jet well. The original MM5V3-predicted wind speed maxima were about 50% smaller than those observed by the RASS profilers, while the modified simulations were able to predict maximum wind speeds that were about 75–90% as high as those observed. Also, the model was able to better predict the timing and duration of the LLJ when FDDA was not used below 1.3 km at night. The vertical structure below the LLJs is not well-simulated in all experiments, due to the poor vertical resolution and insufficient dissipation below 400 m.

- Cloud fraction parameterization needs to be improved in the MM5V3 modeling system. The present MM5V3 formulation tends to overpredict low clouds at high RH (>90%) in the PBL, altering the shortwave radiation that reaches the surface, which, in turn, can significantly affect the photochemical modeling results.
- Uncertainties exist in both observations and model outputs. An accurate estimation of uncertainties among different measurement techniques is critical if such observations are to be used as a basis for model performance evaluation.

Acknowledgements

This research was supported by the New York State Energy Research and Development Authority under agreement number 4914-ERTER-ES99, and the U.S. Environmental Protection Agency under grant number R826731476. The views expressed in this paper do not necessarily reflect those of the supporting agencies.

References

1. Cohn, S.A. and Angevine, W.M.: 2000, Boundary layer height and entrainment zone thickness measured by lidars and wind-profiling radars, *J. Appl. Meteorol.* **39**, 1233–1247.
2. Shafran, P.C., Seaman, N.L. and Gayno, G.A.: 2000, Evaluation of numerical predictions of boundary-layer structure during the Lake Michigan Ozone Study (LMOS), *J. Appl. Meteorol.* **39**, 412–426.
3. Alapaty, K., Pleim, J.E., Raman, S., Niyogi, D.S. and Byun, D.W.: 1997, Simulation of atmospheric boundary layer processes using local- and nonlocal-closure schemes. *J. Appl. Meteorol.* **36**, 214–233.
4. Ku, J.-Y., Mao, H., Zhang, K., Civerolo, K., Rao, S.T., Philbrick, C.R., Doddridge, B. and Clark, R.: 2001, Numerical investigation of the effects of boundary-layer evolution on the predictions of ozone and the efficacy of emission control options in the northeastern United States, *Environ. Fluid. Mech.* **1**, 209–233.
5. Dudhia, J.: 1993, A nonhydrostatic version of the Penn State-NCAR Mesoscale Model: validation tests and simulation of an Atlantic cyclone and cold front, *Mon. Wea. Rev.* **121**, 1493–1513.
6. Grell, G.A., Dudhia, J. and Stauffer, D.R.: 1994, *A Description of the Fifth-Generation Penn State/NCAR Mesoscale Model (MM5)*, National Center for Atmospheric Research, Boulder, CO.

7. Byun, D.W. and Ching, J.K.S.: 1999, *Science Algorithms of the EPA MODELS-3 Community Multiscale Air Quality Model (CMAQ) Modeling System*, U.S. Environmental Protection Agency, Washington, DC.
8. Stauffer, D.R. and Seaman, N.L.: 1990, Use of four-dimensional data assimilation in a limited-area mesoscale model. Part I: experiments with synoptic scale data, *Mon. Wea. Rev*. **118**, 1250–1277.
9. Stauffer, D.R., Seaman, N.L. and Binkowski, F.S.: 1991, Use of four-dimensional data assimilation in a limited-area mesoscale model. Part II: effects of data assimilation within the planetary boundary layer, *Mon. Wea. Rev.* **119**, 734–754.
10. Seaman, N.L.: 2000, Meteorological modeling for air-quality assessments, *Atmos. Environ*. **34**, 2231–2259.
11. Biswas, J. and Rao, S.T.: 2001, Uncertainties in episodic ozone modeling stemming from uncertainties in the meteorological fields, *J. Appl. Meteorol.* **40**, 117–136.
12. Sistla, G., Hao, W., Ku, J.Y., Kallos, G., Lagouvardos, K., Kotrini, V., Zhang, K., Mao, H. and Rao, S.T.: 2001, An operational evaluation of two regional-scale ozone air quality modeling systems over the eastern United States, *Bull. Amer. Meteorol. Soc.* **82**, 945–964.
13. Blackadar, A.K.: 1979, High resolution models of the planetary boundary layer. In: J. Pfafflin and E. Zeigler (eds.), *Advances in Environmental Science and Engineering*, pp. 50–85, Gordon and Breach, New York.
14. Gayno, G.A., Seaman, N.L., Lario, A.M. and Stauffer, D.R.: Forecasting visibility using a 1.5-closure boundary layer scheme in a 12-km non-hydrostatic model. In: *Tenth Conference on Numerical Weather Prediction*, pp. 18–20, American Meteorological Society, Boston, MA.
15. Troen, I. and Mahrt, L.: 1986, A simple model of the atmospheric boundary layer: sensitivity to surface evaporation, *Boundary-Layer Meteorol.* **37**, 129–148.
16. Hong, S.Y. and Pan, H.L.: 1996, Nonlocal boundary layer vertical diffusion in a medium-range forecast model, *Mon. Wea. Rev.* **124**, 2322–2339.
17. Zhang, D. and Anthes, R.A.: 1982, A high-resolution model of the planetary boundary layer – sensitivity tests and comparisons with SESAME-79 data, *J. Appl. Meteorol*. **21**, 1594–1609.
18. Philbrick, C.R.: 1998, Investigations of factors determining the occurrence of ozone and fine particles in northeastern U.S.A. In: *Measurement of Toxic and Related Air Pollutants*, pp. 248–260, Air & Waste Management Association, Pittsburgh, PA.
19. Pagnotti, V.: 1987, A mesoscale meteorological feature associated with high ozone concentrations in the northeastern United States, *J. Air Pollut. Control Assoc*. **37**, 720–722.
20. Walcek, C.J.: 1994, Cloud cover and its relationship to relative humidity during a spring midlatitude cyclone, *Mon. Wea. Rev*. **122**, 1021–1035.
21. Angevine, W.M., Bakwin, P.S. and Davis, K.J.: 1998, Wind profiler and RASS measurements compared with measurements from a 450-m-tall tower, *J. Atmos. Oceanic Technol*. **15**, 818–825.
22. Berman, S., Ku, J.Y. and Rao, S.T.: 1999, Spatial and temporal variation in the mixing depth over the northeastern United States during the summer of 1995, *J. Appl. Meteorol*. **38**, 1661–1673.
23. Moeng, C.H.: 1984, A large-eddy-simulation model for the study of planetary boundary-layer turbulence, *J. Atmos. Sci*. **41**, 2052–2062.
24. Moeng, C.H. and Wyngaard, J.C.: 1984, Statistics of conservative scalars in the convective boundary layer, *J. Atmos. Sci*. **41**, 3161–3169.
25. Moeng, C.H. and Wyngaard, J.C.: 1989, Evaluation of turbulent transport and dissipation closures in second-order modeling, *J. Atmos. Sci*. **46**, 2311–2330.
26. Pleim, J. and Chang, J.S.: 1992, A nonlocal closure model for vertical mixing in the convective boundary layer, *Atmos. Environ*. **26**, 965–981.
27. Zhang, J. and Rao, S.T.: 1999, The role of vertical mixing in the temporal evolution of ground-level ozone concentrations, *J. Appl. Meteorol*. **38**, 1674–1691.

28. Whiteman, C.D., Bian, X. and Zhong, S.: 1997, Low-level jet climatology from enhanced rawinsonde observations at a site in the South Great Plains, *J. Appl. Meteorol*. **36**, 1363–1376.
29. Kaplan, M.L., Lin, Y.L., Charney, J.J., Pfeiffer, K.D., Ensley, D.B., DeCroix, D.S. and Weglarz, R.P.: 2000, A terminal area PBL prediction system at Dallas-Fort Worth and its application in simulating diurnal PBL jets, *Bull. Amer. Meteorol. Soc*. **81**, 2179–2204.
30. Anderson, B.T., Roads, J.O., Chen, S.C. and Juang, H.M. H.: 2000, Regional simulation of the low-level monsoon winds over the Gulf of California and southwestern United States, *J. Geophys. Res*. **105**, 17 955–17 969.
31. Holtslag, A.A.M., de Bruin, E.I.F and Pan, H.L.: 1990, A high resolution air mass transformation model for short-range weather forecasting, *Mon. Wea. Rev.* **118**, 1561–1575.
32. Holtslag, A.A.M., Meijgaard, E.V. and DeRooy, W.C.: 1995: A comparison of boundary layer diffusion schemes in unstable conditions over land, *Boundary-Layer Meteorol.* **76**, 69–95.
33. Willmott, C.J.: 1981, On the validation of models, *Phys. Geogr*. **2**, 168–194.